



Turbulence structure and scales in canopy-wake reattachment

Hayoon Chung * and Jeffrey Koseff 

The Bob and Norma Street Environmental Fluid Mechanics Laboratory, Department of Civil and Environmental Engineering, Stanford University, Stanford, California 94305, USA



(Received 21 July 2021; accepted 15 November 2021; published 30 November 2021)

The reattachment of turbulent flow in canopy wakes is studied in laboratory flume experiments with model submerged aquatic vegetation. Velocity profiles using acoustic Doppler velocimeters were taken in the wakes of homogeneous (single-patch) canopies and within long gaps of discontinuous canopies (two patches). Analysis of the velocity records for mean flow and turbulence statistics suggests the presence of two dominant dynamics and scales: canopy-shear dynamics (CSD) and backward-facing step dynamics (BFSD). The mean streamwise velocities near the bed of the canopy wakes indicate the presence of an adverse pressure gradient, as found in the wake of BFS or other flow expansions. Using this observation, we redefine the reattachment for canopy wakes. Spectral analysis of the streamwise velocity near the bed in the immediate wake of the canopy shows that there is a significant peak centered about a frequency comparable to the streamwise periodicity found in the immediate wake of a BFS. Further from the bed, the vertical velocity spectra maintain a strong spectral peak that corresponds to the coherent structures formed by the canopy-shear instability from the upstream canopy. While different canopy systems have different contributions from the two dynamics, our canopy systems are dominated by canopy-shear dynamics about the canopy height in the wake. For example, CSD has a strong influence on the turbulence in the wake of the canopy because the length of the canopy controls the turbulence development. This in turn has a strong influence on the reattachment length. (However, the BFSD modifies the dominant CSD-induced signal by introducing both larger and smaller scales to the flow.) We find that the reattachment length decreases with increasing canopy length of turbulence, with an asymptotic limit for the canopy length required for fully developed turbulence.

DOI: [10.1103/PhysRevFluids.6.114605](https://doi.org/10.1103/PhysRevFluids.6.114605)

I. INTRODUCTION

Understanding and characterizing the role of submerged aquatic canopies on modifying the velocity fields and local structure of the surrounding flow has been an area of research and interest across many different systems and applications. Studies have focused on the transport of momentum, turbulence, and mass in various ecological systems such as submerged aquatic canopies [1–3], bivalves [4,5], coral reefs [6], terrestrial canopies [7,8], crop fields [9,10], and urban canopies [11,12]. While the focus of most studies has been on the flow development over and through homogeneous lengths of canopies [13] and the impacts of the interactions between the flow and the canopy on sediment transport [14–16], limited attention has been given to flow through heterogeneous canopies, such as those with gaps. Particularly, there is limited understanding of flow behavior near canopy trailing edges and of flow reattachment to the bed in the canopy wakes.

*hayoonch@stanford.edu

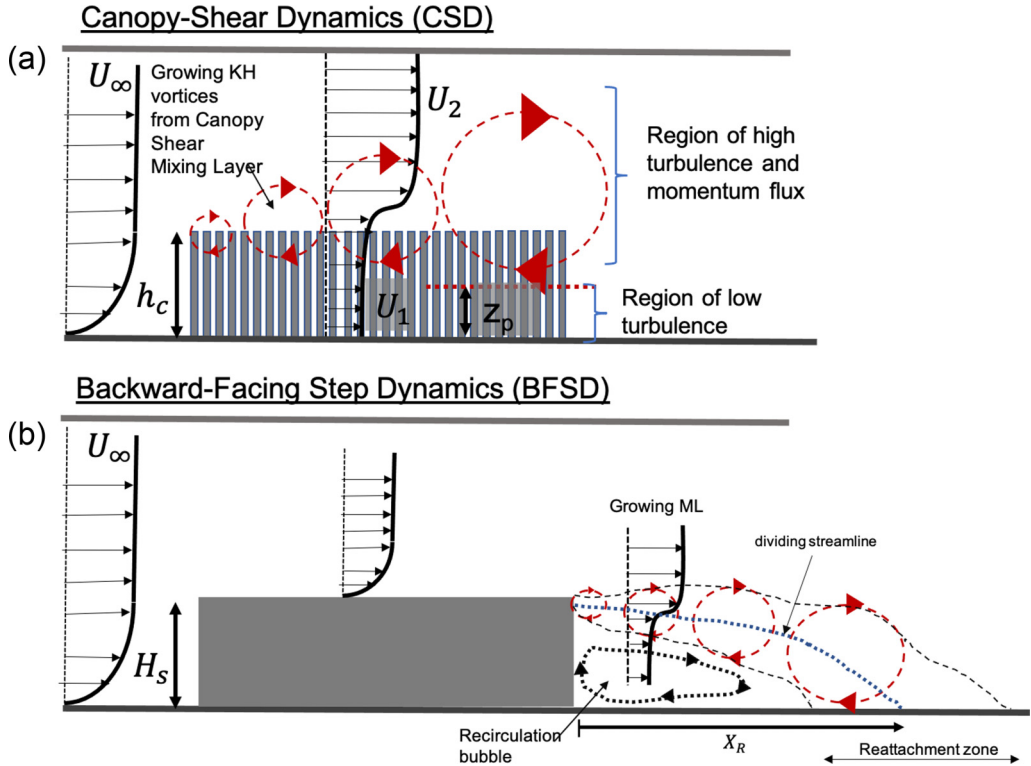


FIG. 1. (a) Schematic of submerged canopy system. U_∞ corresponds to the free stream velocity before the flow interacts with the canopy. U_2 and U_1 correspond to the overflow and throughflow of the canopy mixing layer. (b) Schematic of backward-facing step. X_R is the reattachment point.

Because heterogeneous canopies have multiple edges or ends, we find that it is crucial to understand the characteristics and underlying physics behind the turbulent reattachment in canopy wakes.

In general, flow through aquatic submerged canopies is found to be analogous to the canonical mixing layer (ML) [1,13,17–19]. The vegetation canopy exerts drag on the ambient flow, thereby deflecting the flow above it. If the vegetation density is high enough [$ah_c \geq 0.1$, where a is the frontal canopy area (m^{-1}) and h_c is the canopy height], the streamwise velocity profile over the depth $U(z)$ will develop an inflection point near the canopy height [13]. This flow is susceptible to the Kelvin-Helmholtz (KH) instability, resulting in coherent structures at the canopy-flow interface that control the momentum and turbulence flux into and out of the canopy. These structures, in turn, reach through the porous canopy to a distance z_p from the bed as shown on Fig. 1. The depth of the penetration of the turbulence into the canopy is given by $h_c - z_p$ [17,20]. z_p effectively separates the canopy into an upper layer that is characterized by turbulent shear-scale vortices and rapid changes in mass and momentum transfer, and a lower layer that is characterized by slower changes and limited turbulence.

The lack of vegetation at trailing edges and ends of canopies disrupts such characteristics of canopy flows, leading to flow reattachment to the local bottom and reestablishment of the bottom boundary layer. A subset of studies on heterogeneous or discontinuous canopies have looked at the flow characteristics downstream of canopies [2,21–24] and also within spanwise gaps in submerged canopies [2,3,25–27]. Two types of flow and turbulence characteristic of the canopy wake can be found commonly across many of the studies. First, the transition from canopy to bare bed causes flow separation due to the flow expansion [Fig. 1(b)]. This results in a turbulent wake that greatly

alters the wake dynamics. Second, the turbulence and flow structure characteristic of the canopy-shear upstream [i.e., KH vortices on Fig. 1(a)] also strongly impacts the flow in the wake. The contribution of each of these to the observed turbulence in canopy wakes varies across different studies.

Detto [21] distinguishes these two different flow behaviors for the flow reattachment in forest canopy edges. There are two types of canopy-wake behavior: the “exit-flow” type and the “backward-facing step” (BFS) type. Flow at the trailing edge of a denser canopy will behave like a BFS, while sparser canopies will retain the behavior of the upstream canopy-generated turbulence. Their study distinguishes BFS behavior by the presence of recirculation bubbles in the wake of canopies. In BFS, the adverse pressure gradient at the flow expansion causes the flow separation and reversal in flow direction at the bed that feeds the recirculation cell [Fig. 1(b)]. Such comparison of the behavior of the flow to BFS for canopy edges, and to cavity flow for short gaps [26], seems to hold when canopies are dense enough to influence the flow in the way a solid would. Canopies that are dense enough will form recirculation bubbles in their wakes as the separated flow reattaches to the bed. However, rather than only behaving as either of these two extremes, Detto [21] found that canopies can display properties of both. In particular, even sparser canopies that should be characterized mostly by canopy-generated turbulence display intermittent recirculation patterns corresponding to BFS. Similarly to Detto [21], we find that many previous studies of canopy wakes display both types of behavior, to different extents.

In addition to recirculation, a commonly observed characteristic of BFS-like behavior found by canopy edges is enhanced turbulence, or the presence of a “turbulent wake” by the canopy trailing edge. In a pure BFS, as shown in Fig. 1(b), the flow separation forms a developing shear layer. The turbulence intensity at the “step” height initially increases to a peak that begins approximately one step height upstream of reattachment [28–30], and is then followed by a rapid decay. Such nonmonotonic enhancement and decay of turbulence is also observed in the wake of canopies such as in Folkard’s [2] study of the interaction of a submerged, flexible canopy’s wake with another canopy. Their study found that due to flow separation, a turbulent wake [region of elevated Reynolds stress (RS) and turbulent kinetic energy (*tke*)] formed downstream of the canopy’s trailing edge. Folkard [2] used a length scale L_w to define the “near-wake” and “far-wake” regions and found that the Reynolds stress and turbulence levels at the canopy height increased nonmonotonically with distance downstream to a peak at $x = L_w$ before decaying. However, Folkard [2] finds that no canopy-shear turbulence influenced this wake behavior because the canopy length was too short for coherent KH structures to develop. Therefore, their study falls more at the extreme end of BFS-like behavior in which the wake is dominated by separation dynamics over canopy shear turbulence.

In a related study, Chung *et al.* [27] focused on characterizing the mean flow and turbulence statistics in a discontinuous canopy to understand the impacts of long gaps on producing perturbations both locally (within the gap) and nonlocally (transported). Their study found that perturbations generated in a gap, as characterized by elevated shear and turbulence introduced to the water column, are transported further downstream to impact the flow and turbulence in subsequent gaps. These perturbations, or turbulence enhancements, were similar to the “turbulent wakes” found in Folkard [2]. However in contrast, the canopy system in Chung *et al.* [27] was a submerged rigid canopy system that is characterized by significant canopy-shear turbulence. Their study emphasized not only that the wakes display canopy-generated turbulence, but also that the turbulence development over the upstream canopy has a strong influence on the strength of the wake turbulence. They found that the mean flow and turbulence development over the upstream canopy depends on the canopy length, canopy density, and canopy submergence, consistent with the findings of Chen *et al.* [31] and Hamed *et al.* [32]. Therefore, the RS and *tke* in the gap increases with longer upstream canopies (more developed turbulence), but asymptotes near the “fully developed” length. The length of canopy required to produce fully developed turbulence X_* is the distance along the canopy at which the production and dissipation is balanced. From this length along the canopy, the KH vortices at the canopy top stop growing. As in Folkard [2], our study observed enhanced turbulence in the wake.

However, because the wake is strongly impacted by canopy-shear turbulence, the characteristics of the observed turbulent wake cannot be attributed solely to the flow separation.

Many canopy-edge and gap studies report the presence of a turbulent wake (enhanced turbulence near the canopy edge) [24,26,27,31,33]. However, limited studies distinguish this common behavior based on whether the wake is characterized by the dynamics of BFS or canopy shear, or both. Upon comparing the different studies, we find that despite similarities and common behavior in observed trends in turbulence, there may be discrepancies as to the nature of the turbulence in the wake across these studies. For example, the canopy systems in the studies of Folkard [2] or Maltese *et al.* [3] are short lengths of a pronated flexible canopy that behave like a solid obstacle, or a BFS. The wakes are dominated by separation dynamics with little influence of canopy-generated turbulence from upstream. In contrast, the wakes of canopies in Chen *et al.* [31] and Chung *et al.* [27] are strongly influenced by significant development of canopy-induced turbulence over the upstream canopy. As a result, their turbulent wakes reflect both wake-separation dynamics and canopy-shear dynamics.

For the remainder of the paper, we will refer to flow and turbulence characteristics relating to the two as canopy-shear dynamics (CSD) and BFS dynamics (BFSD). We find that identifying and distinguishing the wake-behavior dependence on either canopy-shear or BFS dynamics is crucial for understanding canopy flow reattachment. Both types of behavior can potentially alter the location of reattachment, as well as the structure of turbulence in regions of the flow surrounding reattachment. The form of turbulence characterizing the near wake has important implications on transport of turbulence, momentum, scalars, and mass at canopy edges, and in canopy gaps. This behavior could potentially impact the fate and transport of larvae and sediment in coral reef communities, or perhaps the spread of disease in crop fields. This behavior is also relevant to the transport of embers across firebreaks or large gaps during forest fires. Firebreaks are large gaps and stretches of canopy purposefully stripped to reduce fuel load and limit fire spread. However, recent extensive high-cost implementations of such breaks have been shown to be ineffective due to inaccurate prediction of fire-spread behavior [34]. Fires have been found to spread right through these firebreaks. We believe that understanding where and how the flow reattaches depending on upwind canopy characteristics, as well as predictive capabilities of wake turbulence that alter fate and transport of embers, will better inform decisions for firebreak design.

Therefore, in order to better understand the interaction between CSD and BFSD and their impact on flow reattachment and behavior, we aim for the following:

- (1) Better define the characteristics of flow “reattachment” downstream of canopy edges, including establishing the reattachment point near the bed as well as the behavior of the flow above the bed near reattachment.
- (2) Clearly determine the different scales that both govern and indicate the presence of the two different dynamical processes CSD and BFSD in separating canopy wakes.
- (3) Analyze the flow structure in different regions of the flow in the near wake to identify dominant physics or scales that govern observed behaviors and contributions to reattachment.
- (4) Assess the impact of canopy turbulence development on the wake reattachment by comparing the wakes across varying lengths of the upstream canopy.

II. METHODOLOGY

The data set and methodology used for this study are the same as those outlined in Chung *et al.* [27]. The experiments were conducted in a recirculating, unidirectional flume of length 720 cm, width 120 cm, and depth (H) of 40 cm. The canopies were modeled by staggered arrays of wooden dowels fixed onto acrylic boards with a canopy frontal area of $a = 0.064 \text{ cm}^{-1}$. The frontal area is given by $a = n_s d$ in which $d = 0.64 \text{ cm}$ is the diameter of the dowel elements, and $n_s = 0.1 \text{ cm}^{-2}$ is the number of dowels per unit area. This density is classified as “dense” [13], which means the density is high enough for the flow profile to contain an inflection point. The canopies spanned the whole width and varied in streamwise length L_1 . The submergence ratio of the canopy was $H/h_c = 40/15$, where h_c is the height of the canopy. We studied two types of wakes: those downstream

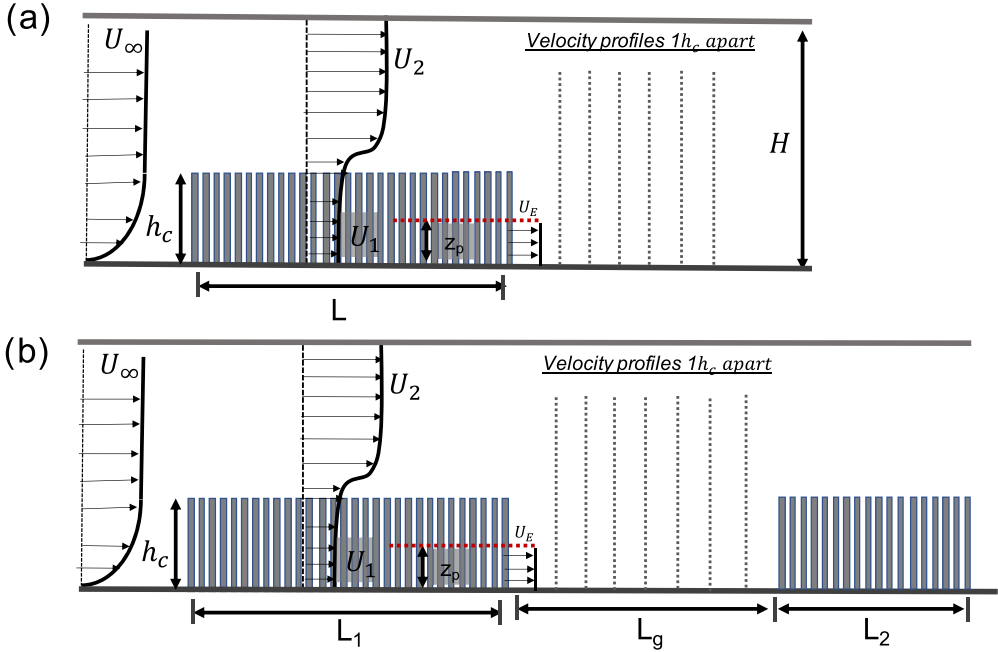


FIG. 2. (a) Schematic of flow over the homogeneous H cases. The canopy height h_c is 15 cm. The water depth H is 40 cm. z_p is the height above the bed to the depth to which the turbulent eddies can penetrate the canopy. U_E is the exit flow velocity, or bleeding flow, in the bottom region of the canopy that is shielded from the canopy vortices. The dotted vertical line provides an example of where velocity profiles were taken. (b) Schematic of flow over the gap, B cases. L_1 , the length of the first canopy is 160 cm, while L_2 , the length of the second canopy, is 120 cm. The length of the gap L_g is listed on Table I.

of a single continuous canopy (homogeneous cases); and those within the gap of a discontinuous canopy (gap cases). For the former homogeneous canopy cases [Fig. 2(a)], we took velocity profiles downstream of a single canopy of varying length L_1 . For the gap cases [Fig. 2(b)], the length of each patch L_1 and L_2 remained fixed at 160 and 120 cm, respectively, while the length of the gap L_g was varied. The chosen cases are listed on Table I.

In this study, two separate flow velocities (flow1 and flow2) were used as listed in Table I. \bar{U} is the depth-averaged velocity and Re is the channel Reynolds number defined by $Re = \bar{U}H_R/\nu$. H_R is the hydraulic radius defined by $H_R = W * H/(2H + W) = 24$ cm. The Re for our flows are 21 600 and 31 200 for flow1 and flow2, respectively. The initial friction velocity u_{*0} is derived from the Reynolds stress at the canopy height ($z = h_c$) at $x = 1h_c$ from the canopy edge: $u_{*0} = \sqrt{-\overline{u'w'}}|_{z=h_c, x=1h_c}$. z_p is the vertical distance from the bed to which the canopy turbulence or vortices from above penetrate, and is approximated as the depth at which the RS falls to about 10% of the maximum RS over the depth. Velocity measurements were taken with an acoustic Doppler velocimeter (ADV) at 200 Hz and low-pass filtered to 50 Hz with a Gaussian filter. Vertical velocity profiles were taken at a number of different canopy height intervals (h_c) downstream of the canopy edge. They were taken up to $6h_c$ downstream for the homogeneous cases and across the whole length of the gap for the gap cases. For each profile, the velocity was measured beginning at 1 to 31 cm above the bed in approximately 4-cm intervals.

For the homogeneous cases we chose canopies of varying length ($L = 120, 160, 280,$ and 480 cm), so that we could compare the development of the turbulence in the wake downstream of the canopy for different canopy lengths. The canopy length required for fully developed canopy turbulence X_* as defined in Chen *et al.* [31], is 375 ± 95 cm for our system. Any canopy lengths

TABLE I. Parameters for homogeneous and gap cases. The table lists both controlled experimental parameters and measured and observed quantities. H stands for homogeneous cases and B stands for the gap cases. The length of the homogeneous canopy or the first patch in the gap canopy is given by L or L_1 . The length of the gap is given by L_g while the length of the second patch for B cases is given by L_2 .

Case	Controlled				Observed		
	\bar{U} (m/s) (flow1; flow2)	L or L_1 (cm)	L_2 (cm)	L_g (cm)	u_{*0} (m/s)	z_p (cm)	X_{R0}/h_c
$H120$	0.09; 0.13	120			0.0081; 0.0112	9.0; 9.0	4
$H160$	0.09; 0.13	160			0.0117; 0.0159	6.5; 7.0	3
$H280$	0.09; 0.13	280			0.0126; 0.0219	5.5; 5.5	2
$H480$	0.09; 0.13	480			0.0146; 0.0220	4.5; 5.0	2
$B80$	0.09; 0.13	160	120	80	0.0115; 0.0183	6.5; 7.0	3
$B120$	0.09; 0.13	160	120	120	.0114; .0174	6.5; 7.0	3
$B160$	0.09; 0.13	160	120	160	.0113; .0178	6.5; 7.0	3
$B200$	0.09; 0.13	160	120	200	.0126; .0178	6.5; 7.0	3

less than X_* will produce lower levels of turbulence by the canopy edge. While the 480-cm canopy has fully developed turbulence, the turbulence levels at the canopy edge for the remaining cases have varying turbulence levels that increase with increasing canopy lengths. In general, the longer canopies introduce higher levels of turbulence to the canopy wake [27].

For the gap cases we fixed the lengths of the upstream and downstream canopies and varied the length of the gaps L_g from 80 to 200 cm. We note that we use the data from the $B200$ gap case to augment the data used for some near-bed analyses in the region just downstream of the $L_1 = 160$ cm ($H160$) homogeneous case. We did this because we found after completing the initial $H160$ study that the flow in this region required a longer signal record for convergence. For the $B200$ study we used 12-min records rather than the 6-min records in the immediate wake of the canopy. The $B200$ case should be indistinguishable from $H160$ for near-bed measurement points in the immediate wake of the canopy because the gap lengths are long enough such that the second canopy will have limited influence on the near-wake dynamics [2,26].

Using the setup and methodology outlined above, we used both velocity records and dye-tracer studies to better understand the mechanism of turbulent reattachment in canopy wakes. Using near-bed trends in mean velocities, we use both traditional and newer criteria to identify reattachment at the bed. Given the highly turbulent nature of the canopy wakes, we analyze the turbulent spectra and relevant scales over both depth and downstream distance to determine the presence of CSD and BFS. Thereafter, to better understand the structure of turbulent mixing, which alters the distribution of turbulence and momentum over the water column and contributes to reattachment, we use quadrant-hole analyses of the velocity records. Finally, we conducted tracer-dye observations in order to visualize how the different regions of the flow (characterized by CSD and/or BFS) interact as they mix.

III. RESULTS

A. Near-bed reattachment in canopy wakes

In this section, we identify the reattachment zones for both homogeneous and gap canopy systems in a systematic way. In Sec. IV B, we discuss the dependence of their location on upstream flow conditions. We consider the reattachment zone to be the region where the turbulent mixing layer that separated from the canopy edge attaches to the bed and the resulting flow begins to form a new boundary layer [35]. In essence, reattachment is defined as the process by which the behavior of a separated free shear layer is increasingly impacted and eventually dominated by a bottom solid boundary. For backward-facing steps (BFS), reattachment occurs when the detached boundary

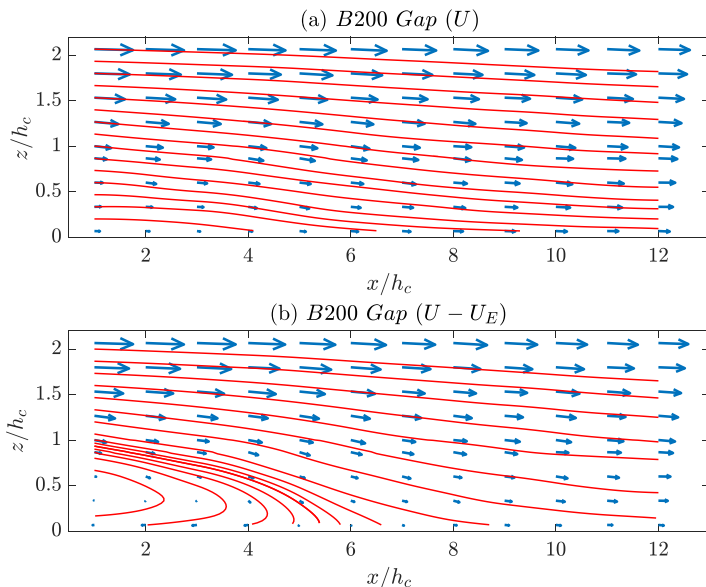


FIG. 3. Vector field (blue) and streamline plot (red) observed in the gap of *B200* for flow2. The x axis is distance from the trailing edge of the canopy patch, normalized by the canopy height. The y axis is the distance above the bed normalized by the canopy height. The top plot (a) is based on mean measured velocities. The bottom plot (b) is based on a modified vector field that is shifted by the exit flow velocity ($U - U_E$).

layer reattaches to the bottom bed at a distance X_R from the step edge. Starting from a distance X_R downstream of the step edge, an adverse pressure gradient drives flow backwards towards the step to feed a recirculation bubble [29,36]. At the “point” of reattachment on the bed surface, the average total shear is small while that above the bed is enhanced through the formation of a shear layer. Therefore, in identifying the reattachment zone it is important to not only identify the point or zone of reattachment at the bed (or in the region of the bed), but also to characterize the flow behavior above the bed (over the water column height) in this zone.

In canopy flows, processes similar to those present in BFS flows modulate the flow separation, with some differences. For example, the recirculation bubble (when present) is displaced further downstream due to the nonzero exit flow velocity U_E from the canopy [2,21,26]. U_E is the depth-averaged flow through the canopy below z_p as shown in Fig. 2(a). Moreover, in canopies that are sparser, while still being dense enough for KH vortices (CSD) to develop, recirculation bubbles may not be present. In such cases, the reattachment point X_R cannot be found using the traditional BFS method for all canopy cases. For our study, we identify the reattachment zone as beginning where (1) near the bed, the adverse pressure gradient forms a significant opposing flow, and (2) over the water column, enhanced mixing allows for more vertical homogeneity in turbulence. We will follow this definition of reattachment for the remainder of the paper. The major difference from BFS reattachment is that the decaying mixing layer in the wake of canopies is influenced by the upstream canopy shear structure and resulting Kelvin-Helmholtz instabilities, and not just by the nature of the separated flow from the BFS edge. Another difference is due to the presence of U_E : the flow only needs to attach to or adjust to the canopy lower-layer velocity rather than to the no-slip condition at the bed. More specifically, the overflow needs to adjust to the exit flow velocity U_E that characterizes the z_p region. Beyond this region, the flow will adjust as the canopy-overflow and throughflow regions in the wake connect into one turbulent shear layer.

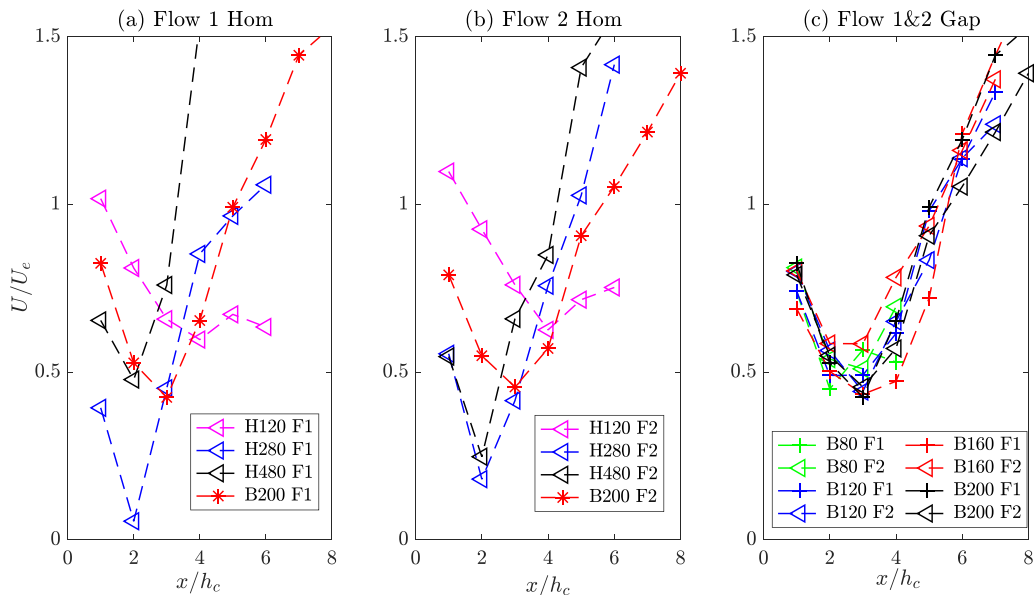


FIG. 4. Streamwise velocity U along the bed at 1 cm above the bed. (a) Velocity measurements downstream of homogeneous canopies for flow1 H cases (and $B200$ for $L_1 = 160$ cm). (b) Velocity measurements made downstream of homogeneous canopies for flow2 H cases (and $B200$ for $L_1 = 160$ cm). (c) Velocity measurements made inside the gap of B cases for both flow speeds.

As presented by the streamlines and vector field in Fig. 3(a), there are no time mean flow reversals or recirculation bubbles in the wake of our canopies. In Fig. 3(a) we plot the vector field in the wake of the upstream canopy for the $B200$ -flow2 case based on measured velocity profiles. This plot shows that in the immediate wake of the canopy ($z/h_c < 1$, $x/h_c < 3$), there is a significant reduction (near zero) of streamwise velocity but there are no flow reversals. This region is referred to as the wake “dead zone” in Zarama [24] and Chung *et al.* [27]. By around a distance of $x/h_c = 5$ to 6, the flow in this dead zone below the canopy height has regained some momentum as the overflow penetrates to the bed. Similar behavior and trends are observed downstream for the other experimental cases (both gap and homogeneous).

In Fig. 3(b) we plot the vector field in a moving frame of reference, by subtracting the mean exit velocity U_E from the vector field. As a result, we observe flow recirculation similar to that found downstream of a BFS. This signifies that while the raw mean flow field does not display any recirculation bubbles, recirculation can be observed in an advective frame. However, these impacts are limited and indicate that the mean flow field does not completely exhibit the same characteristics as BFS flow.

The lack of recirculation may be due to two related reasons. First, because the canopy is quite porous, the adverse pressure gradient is weaker than that in denser canopies such as in Folkard [2] or Hamed *et al.* [26]. This results in a weaker reverse flow. Second, the magnitude of the velocity of the flow exiting the canopy (U_E) is high. As a result, any flow reversal resulting from the weak adverse pressure gradient needs to overcome the opposing U_E to form a recirculation bubble. As a result, while there is no mean backward flow, the magnitude of the streamwise velocity along the bed will reduce to a minimum and, thereby, exhibit a nonmonotonic trend. In Fig. 4 we plot the streamwise velocity U at a height $z = 1$ cm along the bed downstream of the canopy. Figures 4(a) and 4(b) show results for the different homogeneous cases for flow1 and flow2. (Note that the $B200$ flow case was used here in place of the $H160$ case for reasons detailed in the methodology.) Figure 4(c) plots the same for all of the gap cases, for which $L_1 = 160$ cm. U is normalized by U_E , the exit

velocity measured at the immediate edge of the canopy. The x axis is the streamwise position from the canopy edge normalized by the canopy height h_c .

In Fig. 4, we clearly see the trends referred to above. The nonmonotonic trend in streamwise velocity U signifies a region where the adverse pressure gradient acts strongly. Beginning at the canopy edge ($x/h_c = 0$), the flow at the bed exhibits a significant “bleeding” velocity on the order of U_E , and then decreases to a minimum due to the effects of the adverse pressure gradient before increasing and returning to U_E . The minima for canopies of $L_1 = 160$ cm occur at $x/h_c = 3$. The minima for the $L_1 = 280$ and 480 cm cases occur at around $x/h_c = 2$. For $L_1 = 120$ cm, a minimum can be observed at $x/h_c = 4$, but more downstream measurements are needed to confirm it is a global minimum. These results seem to confirm our hypothesis stated earlier that the nonmonotonic trend is caused by an opposing flow near the bed. Rather than increasing monotonically from U_E to a higher velocity as momentum from the overflow reaches the bed, the flow initially slows down, suggesting that there is a flow opposing U_E in the near-bed region. It is highly likely that this backward flow is caused by the separation-induced adverse pressure gradient. The minima in the dimensionless U observed in Figs. 4(a) and 4(b) occur at the location in the streamwise direction with the maximum opposing backwards flow. In effect then, this canopy system can be regarded as having a pseudo-BFS separation with an effective step height of $H_s = z_p$.

In Fig. 4(c), we observe that the location of the minimum is consistent across varying gap lengths L_g for the gap cases. The minimum is found near $x/h_c = 3$ for *B80*, *B120*, *B160*, and *B200* cases. This shows that the location of this minimum is dependent on the upstream canopy length ($L_1 = 160$ cm across all cases) with little sensitivity to the length of the gap. This signifies that the trends that we observe apply to both downstream of homogeneous canopies and inside long gaps. However, this would not apply for cases in which the gap is shorter than the location of this minima.

Based on this near-bed trend, we define the beginning of our reattachment region to be the point starting with this minimum velocity at X_{R0} . BFS studies show that the region of maximum backward flow is approximately half the reattachment length. The reattachment region extends to a streamwise location X_{R1} , where the flow rate is restored to U_E ($U/U_E = 1$). For example, for the *H280-flow2* case, $X_{R0} = 2h_c$ and $X_{R1} = 5h_c$. The region between X_{R0} and X_{R1} is analogous to the region in BFS flows where the shear layer splits near the bed as the flow reattaches. The split shear layer causes part of the flow to deflect upstream to supply entrainment while the remainder continues downstream with a pronounced decrease in eddy length scale [37]. The observed values of X_{R0} are listed on Table I.

A common way of identifying X_R in separated flows is by measuring the forward-flow probability (FFP) along the bed from the canopy edge. In BFS, the reattachment point is characterized by small time-averaged streamwise velocities with instantaneous reversals in flow direction due to turbulent fluctuations [29,35]. Therefore, the FFP is calculated by taking the percentage of instantaneous velocity realizations that are positive (forward flowing) vs negative (backward flowing). X_R would be the streamwise point where FFP at the bed surpasses 50%. In these canopy wakes, the FFP near the bed always surpasses 95%, making this analysis not applicable.

However, despite the high FFP along the bed, the instantaneous velocity signals fluctuate about a nonzero value in a similar manner to that in BFSs. Because of the strong bleeding flow U_E , the velocity fluctuates between stronger and weaker forward flow instead of positive- and negative-flow velocities. Therefore, we looked at the velocity record in an advective frame with respect to the bleeding flow $U' = U - U_E$. This shift gives us a relative velocity by which we can study the pseudoflow reversals. In Fig. 5 we plot this modified form of the FFP for our shifted U velocity records. Because the FFP is quite sensitive to the value of U_E , this plot is more indicative of trends that can be observed with the shift, rather than actual magnitudes or locations of X_R . In this relative frame of reference, we see that the fraction of forward flow over the sampling duration increases roughly linearly between $x/h_c = 2$ to 6. The FFP surpasses 0.5 for the *H480*, *H280*, and *H160* (actually the *B200* case) between 3 and 5 h_c for the flow1 cases and between 4 and 6 h_c for the flow2 cases. The behavior for *H120* is different from the rest of the cases because it is the case in which the mean flow has not fully readjusted to the canopy, in that the

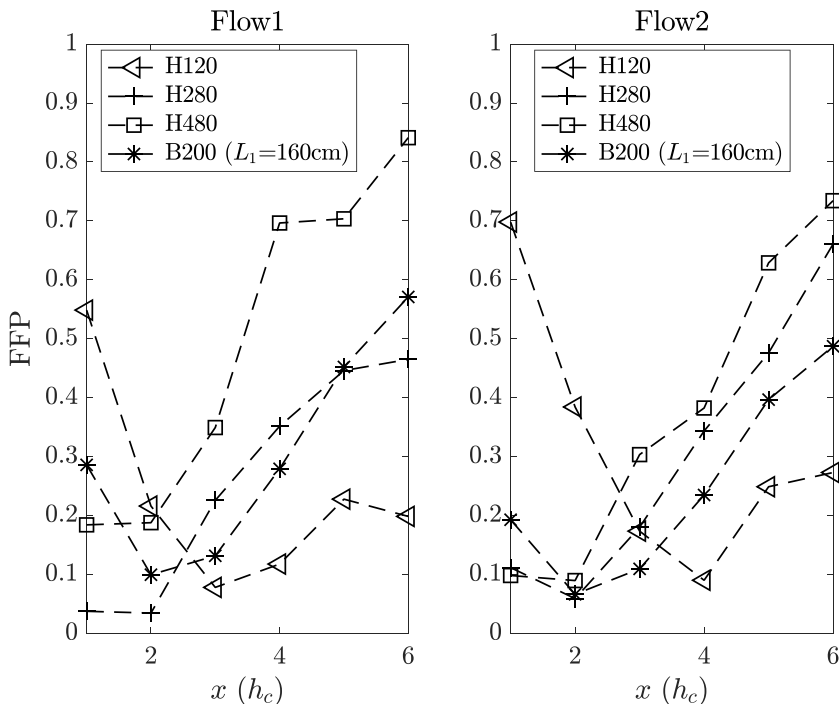


FIG. 5. Modified FFP (forward-flow probability) based on U' along the bed ($z = 1$ cmab) for various homogeneous cases for both flow1 and flow2.

canopy is too short for sufficient canopy drag to slow down the in-canopy flow by the canopy edge.

B. Turbulent scales of CSD and BFS in canopy wakes

In this section, we focus on the different scales that impact the flow, and also on the regions of the flow where such scales dominate. We do this because understanding reattachment requires not only identifying X_R near the bed, but also understanding the turbulent mixing higher in the water column and its contribution to reattachment. Because regions in and near the shear layer away from the bed are heavily influenced by CSD, we need to distinguish between the various scales observable in the wake. The flow through the upstream canopy is divided into an upper layer ($z > z_p$) of high momentum and turbulence (strong presence of CSD) and a lower layer ($z < z_p$) of limited turbulence intrusion [20]. This separation initially persists into the canopy wake [27], but diminishes closer to reattachment through enhanced mixing. Therefore, we use spectral analysis to distinguish regions of the flow that correspond to these “lower” and “upper” regions. We then look for distances at which the regions become less distinguishable, thus indicating flow reattachment. In trying to distinguish markers of CSD and BFS, we identify dominant peaks in the wakes’ turbulence spectra. We identify the characteristics of CSD behavior by comparing observed spectral peaks in the wake to those measured for pure CSD above the upstream canopy. To do this we took separate velocity measurements in the shear layer above the upstream canopy, where only CSD acts on the flow. Results show that by a streamwise distance of 160 cm from the canopy leading edge, coherent structures induced by the canopy display oscillations at $f = 0.13$ s $^{-1}$ and 0.19 s $^{-1}$ for flow1 and flow2, respectively. The presence of these coherent structures appears in the turbulence spectra as sharp, narrow-banded peaks.

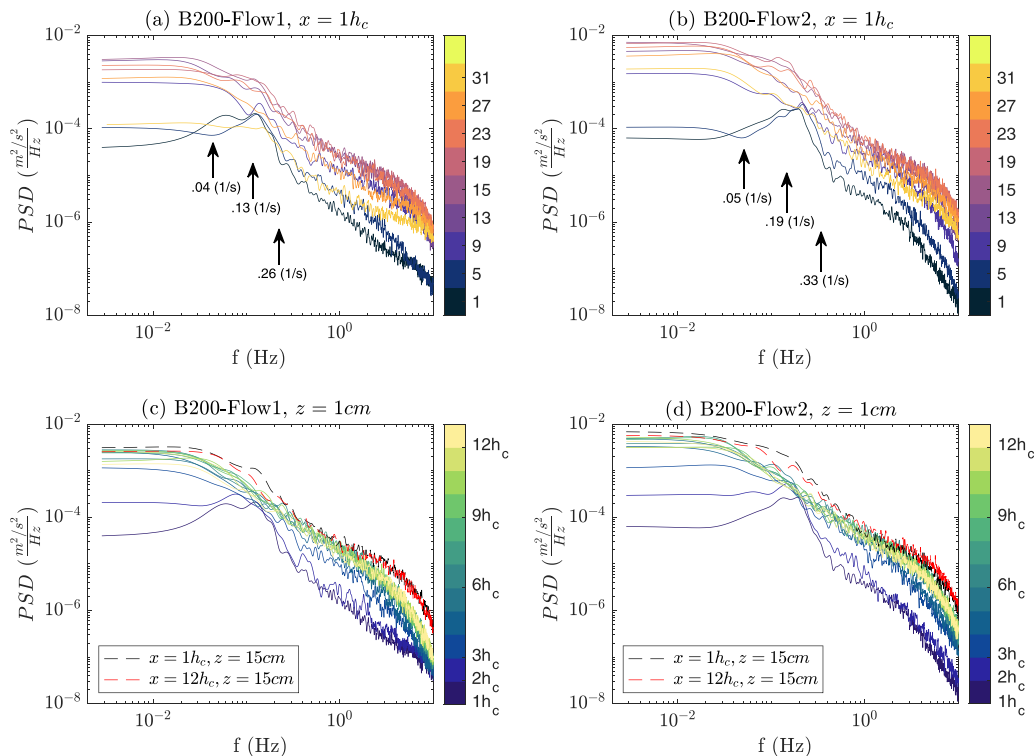


FIG. 6. Streamwise velocity spectra (P_{uu}) at various depths and streamwise distance. (a), (b) Streamwise velocity spectra just downstream of the canopy edge ($x/h_c = 1$), over the whole depth from $z = 1$ to 31 cm above the bed. (c), (d) Streamwise velocity spectra along the bed (1 cm above the bed) from 1 to $12 h_c$ from the trailing edge of the canopy. The black and red dotted lines plot the spectra at the canopy height (at $x/h_c = 1$ and 12) for comparison to a fully turbulent measurement point.

In the near-wake region just downstream of the canopy, the lower region is characterized by the bleed velocity U_E and fairly low turbulence levels, while the upper region contains the upstream canopy-induced turbulence (CSD) that is advected into the wake at the overflow velocity. In Fig. 6, we plot the turbulence spectra for streamwise velocity fluctuations (P_{uu}) in the canopy wake (gap) of the *B200* case. We use *B200* as the representative case here simply because we have measurements up to $12h_c$ in streamwise distance (as opposed to up to $6h_c$ for *H* cases), and wanted to observe trends over longer distances. Spectra downstream of *H* cases, not shown, follow similar trends. In Figs. 6(a) and 6(b) we plot the spectra over the depth of the water column at $x/h_c = 1$ from the canopy edge for flow1 and flow2, respectively. In these plots, the color bar from black to yellow progresses from 1 cm above the bed to 31 cm above the bed. We see that near the bed at ($z = 1$ cm), there are significant peaks at $f = 0.13$ and 0.19 s^{-1} . This measurement point is located within the shielded dead zone in the immediate wake of the canopy, where both velocity and turbulence are limited. Because the flow in this region is not particularly turbulent, we attribute the existence of the peaks to the strong streamwise unsteadiness seen in the immediate wake. This peak in energy is observable also at $z = 5$ cm, but is lost from $z = 9$ cm and higher. This cutoff height is close to the penetration depth $z_p = 6.5$ – 7 cm in the upstream canopy, which is the height to which the shear layer penetrates the canopy. The distinct spectral peak is not present higher in the water column because the increase in turbulence in this region (corresponding to the CSD turbulence from the upstream canopy containing energy at many scales) tends to fill in the spectra over a wide range of scales, thus making any peaks less obvious.

In Figs. 6(c) and 6(d) we plot the streamwise velocity spectra at a height of 1 cm above the bed over a range of distances from the canopy edge (x/h_c from 1 to 12) for flows flow1 and flow2, respectively. The red and black lines, provided for comparison, correspond to fully turbulent spectra from velocity measurements at the canopy height at the beginning and end of the gap. The spectra show that this near-bed region is initially shielded (with limited intrusion of turbulent energy) to about 2 to 3 canopy heights. Thereafter, the turbulence increases and reaches an asymptotic limit. The comparison with red and black lines shows that the asymptotic limit of the near-bed velocity spectra is close to the turbulence level measured at the canopy height. Therefore, by $x/h_c = 3$, the bed experiences the turbulence levels found at the canopy height. Overall, we find that in the immediate wake of the canopy, the lower region (below z_p) is shielded from the canopy's turbulent energy but maintains a strong streamwise periodicity.

The strong Strouhal peak (Fig. 6) corresponding to streamwise velocity fluctuations is detected in the laminar near-bed region of the wake. This behavior is also found in BFS flows. In the region of recirculation near the bed for BFS wakes, low-frequency periodicity in the streamwise velocity spectra can be observed [38–40]. This periodicity, or “flapping,” of the reattaching shear layer is thought to be caused by instantaneous imbalances between the shear layer entrainment of fluid from the recirculation bubble, and reinjection of fluid near reattachment. The streamwise peak frequency identified for our study corresponds to a Strouhal number $St = fz_p/\bar{U} = 0.08$ for both flow cases. [$z_p = 5.5$ cm (for fully developed flow) is used here as the effective step height of our system. \bar{U} corresponds to the depth averaged velocity.] Interestingly, even though this canopy flow is different in significant ways from BFS flows, these Strouhal number values agree with those found in the BFS literature for which $St = fH_s/\bar{U} = 0.077\text{--}0.08$ [29,41].

The vertical velocity spectra behave differently from the streamwise spectra. In Fig. 7 we plot the vertical velocity spectra (P_{ww}) observed downstream of the first canopy patch in the B200 flow case. In Figs. 7(a) and 7(b), we plot the vertical velocity spectra over the depth of the water column at $x = 1h_c$ from the canopy edge. We see that unlike the streamwise velocity signal, the vertical velocity at the bed ($z = 1$ cm) does not display any coherent peaks. There are a lack of vertical velocity fluctuations in a region with significant streamwise fluctuations. However, at 5 cm above the bed, we observe that spectral peaks at $f = 0.13$ s⁻¹ and 0.22 s⁻¹ form for flow1 and flow2, respectively. This peak remains with increasing heights, although weakly at $z = 27$ and 31 cm above the bed. The signal is lost much higher in the water column away from the strong shear region.

In Figs. 7(c) and 7(d) we plot the spectra of vertical velocity spectra at points across the gap for $z = h_c/3$ (where there is initially limited turbulence intrusion from above the canopy height) for flow1 and flow2, respectively. The vertical turbulence spectra begin with low energy, but with a strong coherent peak at $x/h_c = 1$ downstream. With distance downstream, the energy at larger scales fills the spectra and the peak is lost. This further indicates that as we move downstream, the mixing over the water column and corresponding intrusion and entrainment of turbulence introduces increasingly large scales over a broad range but with no strong coherence. In Figs. 7(e) and 7(f) we plot the variation in these spectra in the streamwise direction at the canopy height ($z/h_c = 1$) for distances $x/h_c = 1$ to 12 from the canopy edge. The red and black lines, provided for comparison, correspond to fully turbulent spectra from velocity measurements 1 cm above the canopy bed, at the beginning and end of the gap, respectively. The trends show that observable peaks in the spectra are present for up to around $x/h_c = 3$ and are lost thereafter.

The peak frequencies observed in the wake's vertical velocity spectra are the same as those observed in the shear layer above the upstream canopy (pure CSD) at $f = 0.13$ and 0.19 s⁻¹. This confirms that the dominant periodic motions observed within the shear layer are set by the upstream CSD. However, we further observe that the spectral peak observed in the wake is much more broad banded (although centered about the same frequency) than that observed for pure CSD above the canopy. This introduction of new scales is likely caused by the flow expansion and vortex breakup induced by BFS near the canopy trailing edge. The peak CSD frequencies correspond to $St = f\theta/U = 0.054$ and 0.062 for flow1 and flow2. The θ corresponds to the momentum thickness for mixing layers [42]. U is the numerical average of U_1 and U_2 . We find that our measured peak

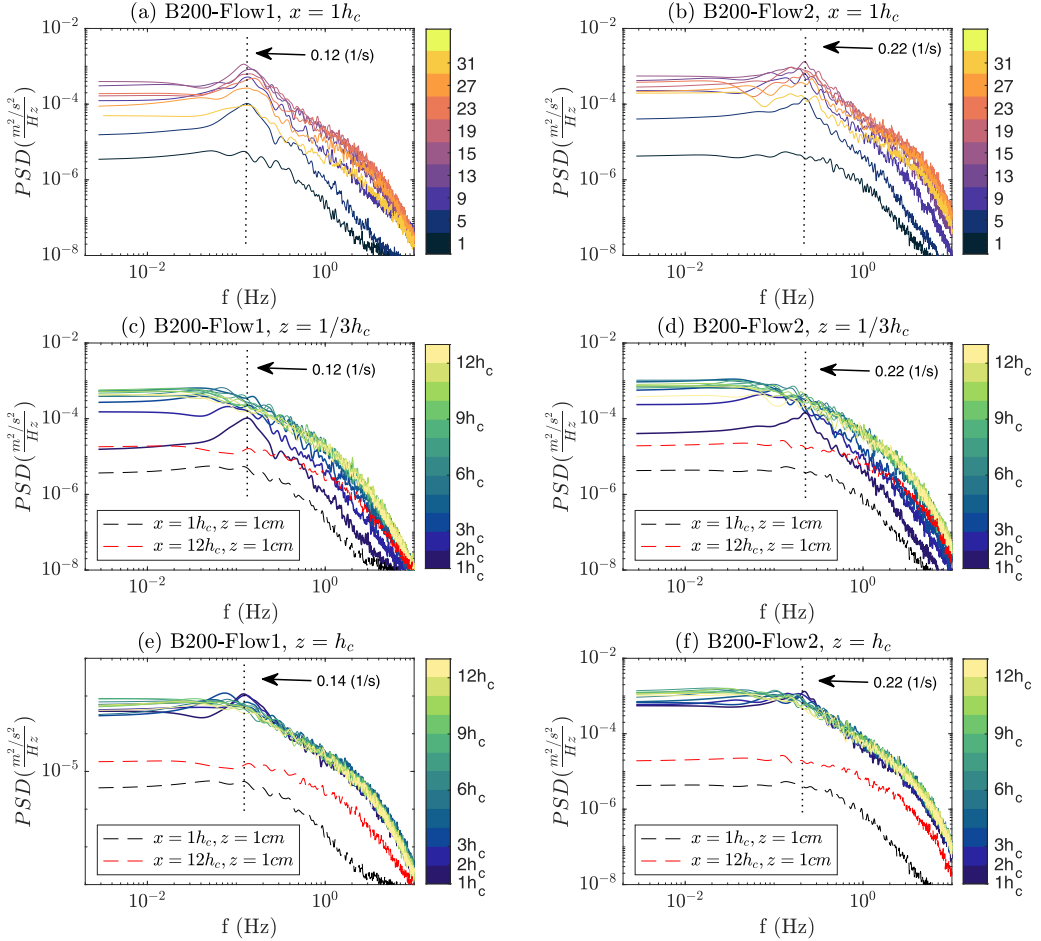


FIG. 7. Vertical velocity spectra (P_{ww}) observed downstream of first canopy patch in B200 case. (a), (b) Spectra observed just downstream of the canopy at $x/h_c = 1$, for depths ranging over 1 to 31 cm above the bed. (c), (d) Spectra observed at $z = 5$ cm over the streamwise distance from $x/h_c = 1$ to 12. (e), (f) Spectra observed at the canopy height over the streamwise distance from $x/h_c = 1$ to 12.

Strouhal is about twice that found for pure mixing layers, $St = 0.032$, by linear stability analysis. While some canopy studies have found measurements that match $St = 0.032$ [17,19], Mandel *et al.* [43] also found a Strouhal peak twice that of the most unstable mode predicted by linear stability analysis. However, although centered at these peak frequencies, the spectral peaks are broad banded and indicate that there is also presence of coherent structures at the frequency predicted by stability analysis [i.e., $f = 0.032U/\theta = 0.076 \text{ s}^{-1}$ (flow1) and 0.11 s^{-1} (flow2)].

Examinations of the vertical and streamwise velocity spectra indicate that the wake is characterized by both CSD and BFS, where the former appears in the vertical fluctuations while the latter can be observed in the streamwise fluctuations. The latter does not imply that BFS is the only way in which near-bed streamwise fluctuation appears in the wake flow. Rather, those points provide a good measure of the BFS scale in a region where there is no influence of CSD. While BFS likely alters the flow throughout the water column, especially in the shear region, it is hard to distinguish exactly between CSD and BFS because their dominant modes are similar. However, we do find that the spectral peaks in the wakes' shear layer (centered about the CSD instability frequency) is much more broad banded than that found for pure CSD above the upstream canopy.

This indicates that BFSF affects the strong CSD signal by introducing a wider range of scales to the flow. Therefore, we hypothesize that while the CSD plays a strong role in setting the dominant frequency contributing to the wake’s turbulent mixing, the BFSF reduces the strength at the peak CSD scale and spreads it to adjacent scales.

C. Turbulent flow structure: Conditional sampling of RS

As indicated by the spectra, the turbulent mixing (which contributes to reattachment) that is centralized about the canopy height is dominated by CSD. However, because utility of the spectra is mostly for comparing frequencies and not for deducing information about the flow structure, we focus here on analysis of the turbulence structure and compare it to that in canopy systems (CSD). We analyze the coherent flow structures that influence the turbulence spectra by conducting a quadrant hole analysis on velocity records. This analysis involves classifying instantaneous Reynolds stresses (RS) by the signs of the velocity fluctuations. The quadrant classifications include (Q1) outward interaction ($u' > 0, w' > 0$), (Q2) ejection ($u' < 0, w' > 0$), (Q3) inward interaction ($u' < 0, w' < 0$), and (Q4) sweep ($u' > 0, w' < 0$). Through this classification, we can conditionally sample the time record and recalculate the mean Reynolds stress based on only contributions from the chosen quadrant(s). Furthermore, this conditional sampling can be focused by setting a “hole” size, by which only events greater than a certain threshold are used to calculate the mean RS. In our analysis we use the threshold defined in Zhu *et al.* [9], given by

$$H_\tau = \frac{|(u'w')_{\text{threshold}}|}{|u'w'|}. \quad (1)$$

By setting the hole size H_τ , which typically spans from 0 (no size filtering) to 5 (filters out RS events that are less than five times the total mean RS), we can isolate the larger or more extreme events that make up the total RS.

Turbulent flows are typically dominated by events from the “sweep” and “ejection” quadrants. Sweeps are turbulent events in which high-momentum fluid sweeps down into a region of low momentum. Ejections are turbulent events in which low-momentum fluid is ejected upwards into a region of high momentum. The dominance of either quadrant is often used to characterize the coherent eddies in organized flows such as boundary layers, mixing layers, and canopy flows. Past literature has shown that in flow through canopies, the flow above the canopy is dominated by sweeps while the flow below the canopy is dominated by ejections [8,19]. It is important to characterize these coherent motions in the canopy wakes to understand reattachment. This is because in the absence of the canopy wakes, sweeps will play a large role in transporting high-momentum fluid down into the gap to the bed, while ejections will transport low-momentum fluid in the dead zone of the canopy wake upward into the turbulent shear layer. Both of these turbulent events will allow for mixing and interaction of the initial two-layer flow in the canopy wake, thus contributing to reattachment. To measure the presence of either of these coherent motions, we use ΔS , a metric for characterizing the dominance of sweeps or ejections for a velocity record:

$$\Delta S_{H_\tau} = S_{Q4,H_\tau} - S_{Q2,H_\tau} = \frac{(\overline{u'w'})_{Q4,H_\tau} - (\overline{u'w'})_{Q2,H_\tau}}{\overline{u'w'}} \quad (2)$$

which, given a hole size H , compares the contribution of sweeps versus ejections to the total Reynolds stress. The numerator in Eq. (1) is the difference in the RS magnitudes for sweep and ejection events that are greater than the threshold. This term is then normalized by the total RS. ΔS_{H_τ} ranges between -1 and 1 , where $\Delta S_{H_\tau} > 0$ is sweep dominated, $\Delta S_{H_\tau} < 0$ is ejection dominated, and $\Delta S_{H_\tau} = 0$ is nonpreferential.

In Fig. 8, we plot various conditional RS magnitudes and ΔS_3 against downstream distance for flow in the gap for the *B200-flow2* case. The ejection (blue) and sweep (black) magnitudes are provided for a hole size of $H_\tau = 3$ (triangle). ΔS_3 is plotted in red with the scale shown on the right-hand axis. Figure 8(a) shows that shortly below the canopy height ($z = 9$ cm), the large scales

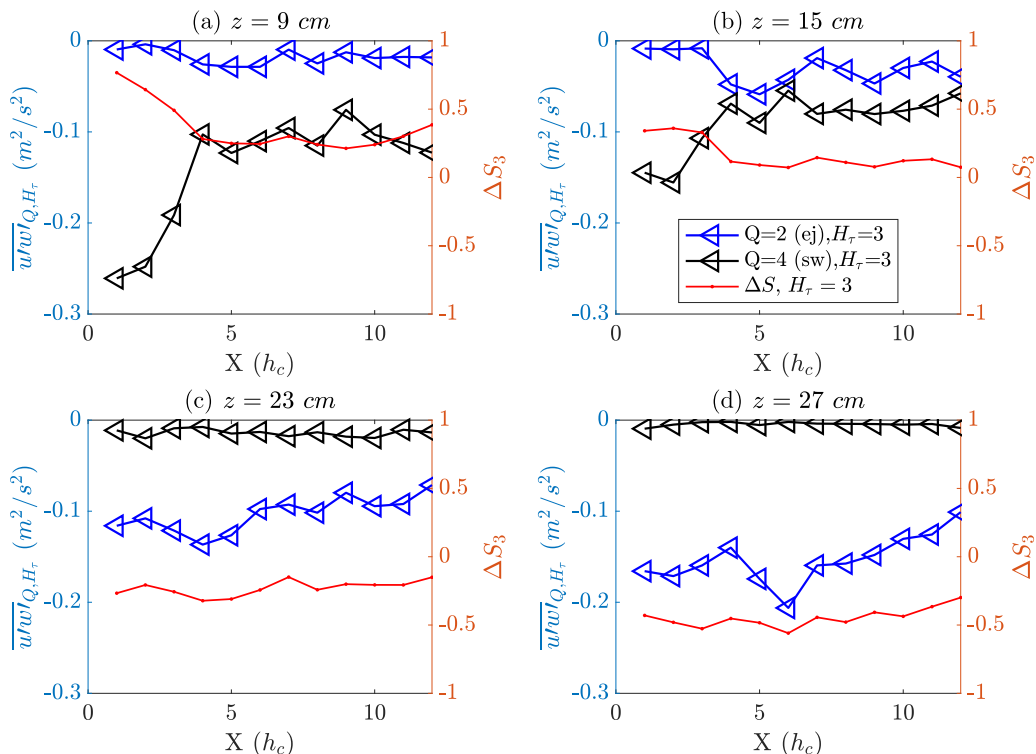


FIG. 8. Results of quadrant hole analysis for velocity measurements in the wake of the first canopy for *B200-flow1* case. The blue and black lines follow the left-hand-side axis for measurements of RS magnitudes for Q2/ejections (blue) and Q4/sweeps (black). The triangle patterns are larger ejection and sweep events of hole size 3. The red line corresponding to the right-hand-side axis is difference in sweep vs ejection contributions to the total RS. Each plot is at different heights.

of the flow are sweep dominated ($\Delta S > 0$), but to a decreasing extent with downstream distance until $x/h_c = 4$, where it plateaus. The RS magnitudes for large events (triangles) show that the ejections remain limited and unchanging while the number of large sweep events tends to decrease with downstream distance.

At the canopy height [Fig. 8(b)], ΔS shows that structures are mostly nonpreferential but initially start slightly sweep dominated. The RS magnitudes filtered for large events ($H = 3$) show that the ejections start near zero but increase slightly beginning at about $x/h_c = 3$ and plateaus shortly thereafter at about $x/h_c = 4$. The sweeps begin with a significant magnitude before decreasing to a plateau, also at about $x/h_c = 4$. At both elevations in the flow above the canopy height [Figs. 8(c) and (d)], the structures are ejection dominated, and there are few large-scale sweep events through the whole length of the gap. The ejections, however, remain significant throughout. The number of large ejection events at $z = 27$ cm (which is close to $\frac{3}{4}$ of the water height) suggests that large-scale ejections from the canopy can reach this height in the water column.

This analysis finds that the turbulent structure in the immediate wake of the canopy matches that found for flow through the canopy. This implies that the matching peaks (corresponding to CSD) in the spectra are supported by matching coherent structures. However, a short distance downstream, the wake flow slowly becomes more nonpreferential and loses resemblance to CSD. The most rapid evolution (with distance from the canopy trailing edge) to a nonpreferential state is observed in the region just below and near the canopy height. As seen in Fig. 8(a), the sharpest decrease in ΔS occurs by $x = 4h_c$ for $z = 9$ cm. This rapid change is mostly caused by a drop in large sweeping

events. At the canopy height ($z = 15$ cm), as shown on Fig. 8(b), the change in ΔS is less drastic. This is because while the sweep events decrease with downstream distance, ejection events increase around $x = 4h_c$. In contrast, the regions far up in the water column ($z = 23$ and 27 cm) display no trends. This difference suggests that the flows at these locations (higher in the water column) are shielded from the dynamics of the rapid mixing observed from the canopy edge about the canopy height. It appears that the upstream canopy was long enough for the rollers to develop and allow for the sweeps to be dominant in the flow at these heights. However, because the vertical extent of the turbulent mixing at the canopy edge does not extend to these heights, the flow continues to maintain its structure. We speculate that the RS at these heights will decay through dissipation with downstream distance and the flow will take much longer to approach a nonpreferential structure. We do not include conditionally sampled RS measured near the bed because while hypothetically influenced by BFS, many of the measurement points are laminar and offer little information with quadrant hole analysis.

Most interestingly, the streamwise location where ΔS plateaus near the canopy height ($z = 9$ and 15 cm) falls within the reattachment zone approximated in Sec. III A, suggesting that above the reattachment zone at the bed, the flow structure stops changing rapidly. Therefore, we hypothesize that most of the large-scale mixing through large ejections and sweeps occurs before and within the reattachment zone. Thereafter, the flow relaxes and readjusts to the bottom boundary and begins to redevelop the boundary layer. This rapid mixing, however, mostly impacts the flow near the canopy height and near the interface between the upper and lower layers (z_p).

D. Turbulent mixing between two layers: Dye study

Both the spectra and quadrant hole analysis indicate that the flow in the canopy wake is initially separated into a region that is dominated by CSD and a region that is dominated by BFS. With distance downstream, the two layers interact through ejections and sweeps, becoming less distinguishable and eventually reattach to the lower boundary. Although the velocity measurements do suggest the form and scales of the flow structures in different regions of the wake, they cannot alone provide a full picture of how the top overflow is mixed and incorporated into the bottom layer. Therefore, we conducted flow visualization with the goal of matching the coherent structures observed in the flow with the output of the spectral and quadrant analyses described in previous sections.

The dye study was conducted as described in Chung *et al.* [27]. Two dye sources of different color were released in continuous streams near the canopy end at two heights. A blue dye was released below z_p , while a green dye was released at the canopy height. This is seen in Figs. 9(a) and 9(b), which display two separate sequences of the flow over two different time periods. The dye visualization displayed here is for the B80g ($L_1 = 160$ cm and $L_g = 80$ cm) setup at the flow2 speed. In each of the sequences each frame is 1.7 s apart. The sequence shown in Fig. 9(a) provides visualization of the flow when the mixing is vigorous and large coherent structures are active. In contrast, the sequence shown in Fig. 9(b) shows the flow during a period of weaker mixing with less visible coherent structures. The two sequences are quite typical of the flow and can be observed repeatedly over the duration of the dye study.

The sequence of frames in Fig. 9(a) displays the passage of a structure generated at the canopy interface over a 5-s period. The red arrows point to such a structure as it begins just downstream of the trailing edge of the upstream canopy in the first frame. It reaches the leading edge of the second canopy by the last frame. During this time the structure (green) has grown in size, and the interaction between the blue and green dyes shows entrainment of the lower layer into the upper layer. We also see in the first frame that there is an older structure that has reached the second canopy, and in the last frame a new structure has begun forming at the upstream canopy edge [black arrows in Fig. 9(a) frames 3 and 4].

In both Figs. 9(a) and 9(b), we see that while the flow is separated into distinguishable streams at the canopy edge, the two layers interact through the actions of the coherent structures with

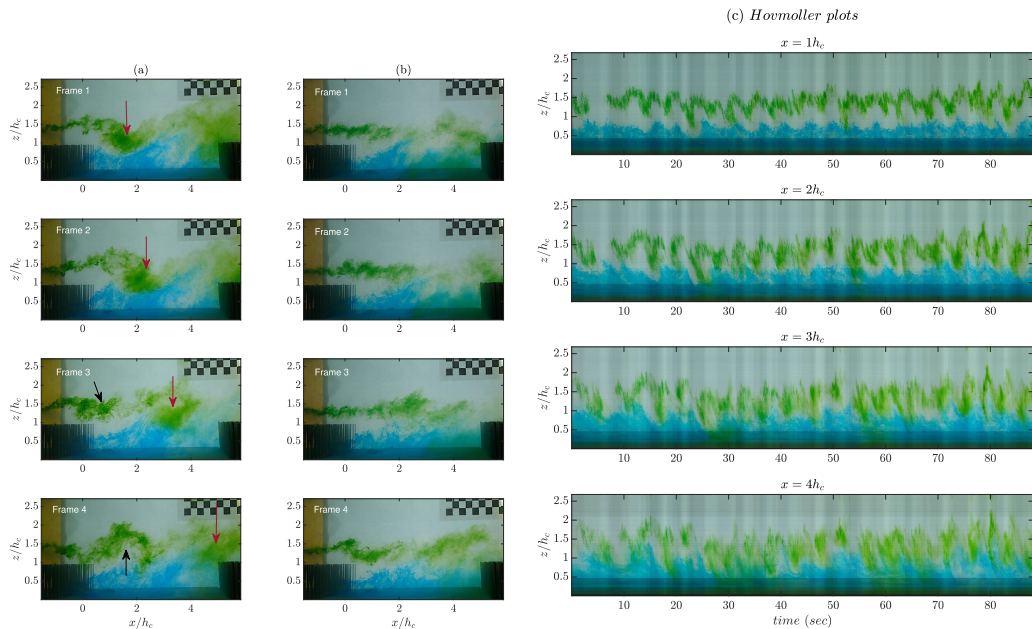


FIG. 9. (a), (b) Sequence of images from flow visualization at two different times. Each subsequent image (top down) is 1.7 s apart. Flow is from left to right, set at flow2 for *B80*. (c) Hovmöller plots over a 90-s sample of the flow visualization videos for distances 1 to 4 h_c from the canopy trailing edge. The depth is normalized by canopy height and the x axis is time in seconds.

distance downstream. Entrainment occurs as the structure in the top layer penetrates the lower layer and engulfs fluid from the lower layer. In Fig. 9(a) frames 1 and 2, ejection (upward transport) of the lower blue fluid can be seen in the underside of the structures in two locations: between $x/h_c = 1$ and 2, and also between $x/h_c = 3$ and 4. Flow visualization downstream of a homogeneous canopy of $L_1 = 160$ cm shows similar behavior of flow structures.

To analyze the scales of the periodicity observed in the record, we plot Hovmöller diagrams at various locations within the gap over a 90-s sample in Fig. 9(c). To create the Hovmöller diagram, we take a profile of pixel values over the depth of the water column (vertical slit of 1 pixel width) at a given streamwise distance. When these profiles are plotted against time, a Eulerian view of the dye pattern at a single streamwise position can be obtained.

The Hovmöller diagram reveals that there is a strong periodicity observed in both the upper (green) and lower (blue) layers. At $x = 1h_c$, there is limited interaction between the two layers while at $4h_c$, there is more intrusion of the top green dye into the lower region toward the bed through the sweeping motions. The blue dye initially fluctuates between $z/h_c = 0.5$ and 1 at $x = 1h_c$, but begins to fluctuate above $z/h_c = 1$ by $x/h_c = 3$ and 4.

To analyze the signal given by the tracers, the green dye is separated from the blue dye as shown in Figs. 10(a) and 10(b). We tracked the vertical position of the green dye record (midpoint between the top and bottom dye/background interface) and the top edge of the blue dye for spectral analysis of the vertical fluctuations. Taking a time record of this dye position and height, we computed the power spectral densities. As shown in the PSD plots in Fig. 10(c), there is a strong peak centered about $f = 0.17\text{--}0.19$ s^{-1} for the bottom layer (red circle), while in the upper layer there is a broader peak spanning from about $f = 0.12$ to 0.25 s^{-1} (blue circles). We find these peaks to be consistent with those found for the velocity measurements of the *B80*-flow2 case (same case as in dye visualization). Near the canopy height in the gap, the velocity spectra show a peak at $f = 0.15$ s^{-1} (P_{xx}) and $f = 0.2$ s^{-1} (P_{zz}), similar to that observed in Figs. 6 and 7 for *B200*. The

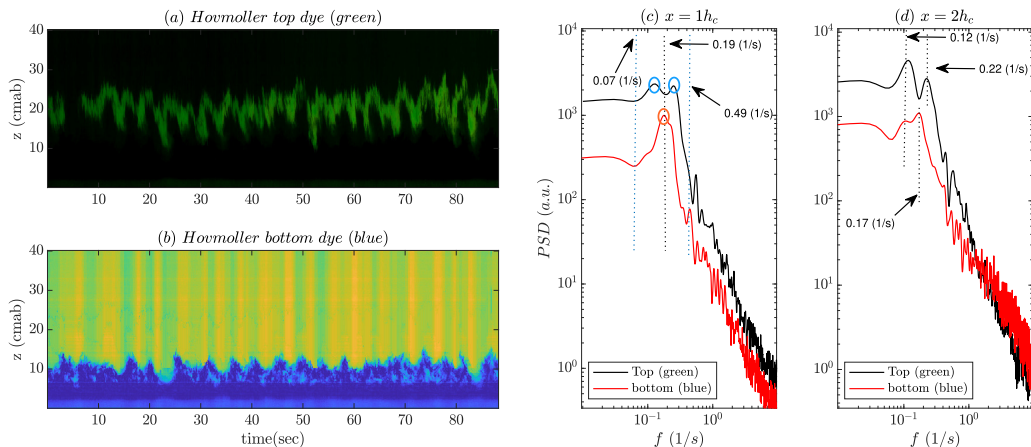


FIG. 10. (a), (b) Example of the Hovmoller plot with just the green dye (top) and blue dye (bottom) isolated. (c), (d) Spectra of the fluctuations in position of the dye for either the green or blue dye. Spectra are based on the position of the midpoint (over the depth) of the green dye and based on the upper limit of the blue dye. The blue circles correspond to $f = 0.12$ and 0.25 s^{-1} . The red circles correspond to $f = 0.17$ – 0.19 s^{-1} . The spectra presented here are for the signal at $x = 1$ and $2h_c$.

broader peak observed in the dye spectra, as for velocity spectra, may indicate more varying large scales as a result of competition and interaction between the CSD and BFS. This confirms that the coherent structures observed in the flow visualization match the periodic structures induced by the upstream canopy that characterizes the mixing dynamics in the reattaching flow.

The PSD plots in Figs. 10(c) and 10(d) show that the spectral peaks in the time records of the top and bottom layer dye match at $x = 1h_c$ and $2h_c$. This corresponds to the initial region of the wake where there is limited mixing between the two layers. As shown in the Hovmoller plots in Fig. 9, there is little intrusion of the top layer into the lower. However, the unsteadiness in the two layers seems to be synchronized and they fluctuate with the same periodicity. This suggests that while there is no mixing and the layers remain separate, the interface fluctuates vertically up and down at the frequency set by the canopy instability. Thus, even though it is shielded from mixing and the turbulent structure of the overflow, the variability in the flow in the bottom region close to the interface is modulated by the top layer's periodic motion.

This observation is supported by the velocity record in the region of $z = z_p$, where both the streamwise and vertical velocity signals display periodic peaks. The streamwise velocity spectral peak corresponds to the separation-induced flapping while the vertical spectral peak corresponds to this fluctuating interface. Further downstream, such as at $x/h_c = 3$ or 4 , there is less distinction between the green and blue dye [Fig. 9(c)]. This is the distance downstream where more mixing and entrainment of the lower layer breaks down the interface between the two layers. This agrees with observations of the velocity spectra in Sec. III B, in which we found that the distinct frequency signal in the streamwise direction near the bed is lost by $3h_c$ downstream. The location where the green dye penetrates more into the lower (blue) region corresponds to the location where there is higher turbulent energy near the bed. This indicates that these CSD-generated large-scale structures we see in the flow visualization are responsible for setting both the momentum and turbulence levels at the bed. As a result, they contribute both to the establishment of the reattachment zone at the bed, as well as the dynamics of the entire water column in this region.

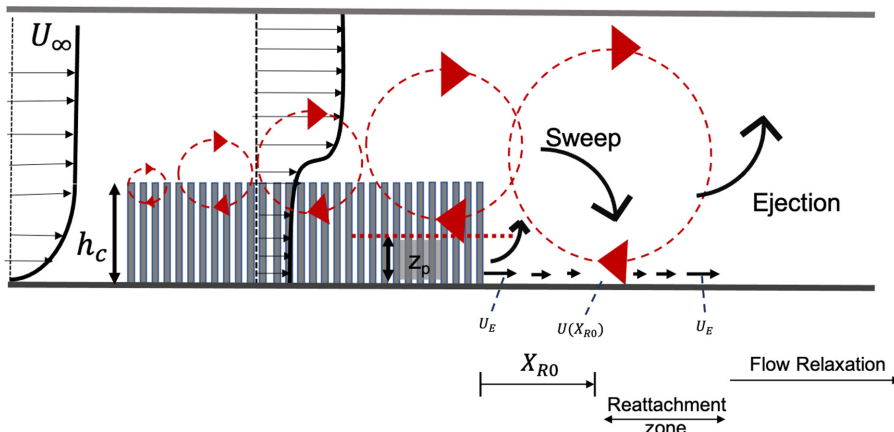


FIG. 11. Schematic of turbulent flow reattachment in canopy wakes. The coherent canopy-induced instability (due to CSD) develops over the canopy and advects into the downstream wake and interacts with BFS. The expansion of the KH rollers, as well as the impact of the BFS separation on the flow, introduces a range of new scales to the system, while maintaining the dominant scale of CSD. The wake is characterized, with downstream distance, by regions of alternating ejection, sweep, then ejection that occur periodically. These periodic coherent fluid motions characterize the turbulent mixing between the upper and lower portions of the water column, thereby contributing to the reattachment dynamics (located at X_R along the bed).

IV. DISCUSSION

A. Comparison of canopy wakes to BFS

The various results presented in the previous section helps our understanding of the different components of flow reattachment in turbulent canopy wakes. The trends in mean flow allow us to locate the distance from the canopy edge at which reattachment occurs at the bed, similarly to BFS. However, due to the strong role of CSD in the turbulent mixing over the water column, we looked more closely at the relevant scales and flow structure above the reattachment point. We found that while the CSD set by the upstream canopy remains the dominant character in the wake (by setting the peak frequency in spectra and setting the turbulence structure), the BFS modifies the CSD by introducing newer scales adjacent to the peak frequency and causing rapid decay of preferential turbulent structure. Therefore, we find that a modified form of CSD turbulence plays a large role in establishing where the reattachment of the canopy shear layer occurs. This interaction manifests itself in the wake, where we observe that initially, a shielded “dead zone” in the wake of the canopy exists where the effects of CSD are diminished. Thereafter, the intrusion of momentum and turbulence from the canopy shear layer to the bed allows for the flow boundary layer to slowly redevelop.

The role of CSD in strongly characterizing the turbulent mixing in the canopy wake sets apart canopy ends from BFS. A key distinguishing property of a canopy wake is the growth of the shear layer at its trailing edge. As seen in Fig. 1(b), the shear layer in BFS grows from a single point at flow separation. This shear layer, and corresponding turbulent production, grows with distance to X_R while being centered about the dividing streamline. Entrainment occurs at the edges or interfaces of the shear layer where ambient irrotational fluid is drawn in. This process leads to eventual reattachment once all of the reverse flow (due to the adverse pressure gradient) is entrained into the shear layer [38].

However, in contrast to BFS, the canopy wake begins with a developed shear layer. As seen in Fig. 11, the flow entering the wake is not only characterized by well-developed mean mixing-layer (ML) profiles, but also contains well-developed turbulent structures. Because these structures are already well developed, the growth of the shear layer as the flow enters the wake is less meaningful

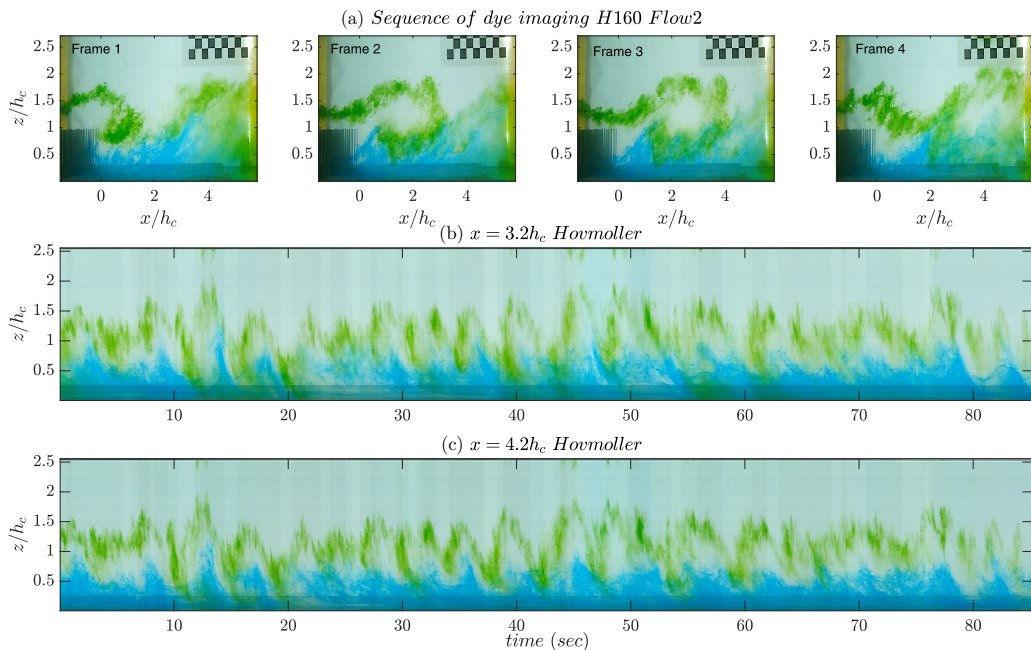


FIG. 12. (a) Sequence of frames from flow visualization for *H160-flow2*. Each frame is 1.7 s apart. (b), (c) Hovmoller plot for sample time range at $x = 3.2h_c$ and $4.2h_c$ from the canopy edge.

in comparison to the scale of mixing that occurs. Rather than a slowly growing shear layer with small amounts of entrainment (“nibbling”) at the interface, the large rotational structure acts at a scale larger than the canopy height, thereby engulfing and mixing the dead-zone fluid into the canopy shear layer. This can be observed in the flow visualization sequence for the *H160-flow2* case shown in Fig. 12(a). In the video frames, similarly to what was observed also in Fig. 9, we can see a shear-layer structure from the canopy in green. This structure sweeps toward the bed, while also entraining fluid from the lower layer (blue). This shows that fluid from both sides of the mixing layers reaches far past their initial bounds.

Such trends are similar to the observed behavior of entrainment in the high Reynolds number turbulent ML dye studies of Dimotakis and Brown [44]. In their study of entrainment, it was found that freshly entrained irrotational fluid penetrates well into the turbulent layer. The fluid from one side can “cross” all the way into the other layer and stay distinguishable until small-scale processes mix them together. This is similarly observed for our study in Fig. 12(a). On the first frame of the flow visualization snapshots, a streak of blue dye originating from the bottom layer extends above the canopy height into the water column at around $x = 4h_c$. Furthermore, in the Hovmoller plots [Figs. 12(b) and 12(c)], we can see the distinct green and blue dye streaks extending both far toward the bed and above the canopy height in the water column. This indicates that the passing structures both impinge into the lower region of the flow, as well as entrain and “pull” up the near-wall fluid up higher into the water column. This entrainment and “entanglement” [45] of fluid, which is strongly impacted by CSD in our system, is responsible for the mixing in the wake and ultimately leads to flow reattachment. We speculate that the ejection and sweep events, as observed in the quadrant hole analysis, is the mechanism by which the fluid in the lower and upper portions of the flow is able to exchange with each other. While this process occurs periodically, as modulated by the CSD instability, when averaged over time, we are able to see the trends previously outlined in Chung *et al.* [27]. Specifically, their study observed that the mean flow profile evolves by beginning with a ML entering the gap and turning into a linear shear layer, which steepens with downstream distance to

begin reforming the boundary layer. In the case of the turbulence (*tke*) profiles, the turbulence that is initially concentrated about the canopy height can spread over the whole water column, becoming more uniform with downstream distance. Although expedited by the canopy shear-induced mixing, this trend in mean flow properties is similar to BFS separation in which its ML profile eventually relaxes after reattachment to redevelop the boundary layer.

B. Influence of upstream canopy length on reattachment

Because CSD has a large role in turbulent mixing, and thereby reattachment, in canopy wakes, we assess the impact of turbulence development on the point of reattachment. We do this by comparing the wakes across varying lengths of the upstream canopy. Many experimental studies of BFS have found that the effect of the initial turbulence condition (in the boundary layer at the step edge) has a negligible effect on establishing the reattachment point. While some studies have hypothesized that higher turbulence levels will enhance the entrainment of fluid into the shear layer, and thereby shorten the reattachment [37,46], other studies have found that the growing shear layer at separation “drowns out” any influence of the turbulence initial conditions [35,36]. Other parameters, such as step aspect ratio, were found to have a greater impact [38]. For canopy wakes, however, the incoming turbulence levels do have a great impact on the reattachment dynamics and location of the reattachment zone. This is because the turbulence levels are associated with the coherent structures that modulate the mixing and interaction of the wake’s two-layer flow. Therefore, we examine these effects and their impact on flow reattachment in our study.

The “initial turbulence condition” in our system refers to the extent to which the shear and turbulent structure develops over the length of the upstream canopy. The distance along the canopy where fully developed mean flow is achieved, X_D , and the distance for fully developed turbulence, X_* , affects the shear scale and turbulence scales by the canopy end [31]. For our canopy systems, all cases except for $H120$ are longer than X_D . In other words, the mean streamwise velocity profiles by the trailing edge are fully developed and have the same shape across the different canopy lengths. In contrast, for turbulence development, only the $H480$ flow cases display fully developed turbulence by the canopy end.

Thus, because we observed that the CSD-induced turbulent structures have large roles in mixing and reattachment in canopy wakes, it is not surprising that we find that canopy lengths have an impact on reattachment. As introduced in Sec. III in Fig. 4 and listed on Table I, X_{R0} varies with different upstream canopy lengths. Two of the longer cases, $H280$ and $H480$, reattach by $x/h_c = 2$, but the cases with $L_1 = 160$ cm ($B80$, $B120$, $B160$, $B200$) only reattach by $x/h_c = 3$. The difference across these cases is that $H280$ and $H480$ are closer to “fully developed” turbulence by the canopy edge than the other cases, and thereby introduce stronger turbulence intensities to the region downstream of the canopy [27]. Although our data are not extensive enough to be definitive, it does appear that higher levels of turbulence and larger coherent structures (corresponding to longer canopies) from the upstream canopy impact and influence the mixing and therefore shorten the reattachment length in the canopy wake. In contrast to BFS where the shear layer and turbulence just begin to develop and grow at the canopy edge, our system is very strongly modulated by the canopy structures that dominate the wake’s mixing and transport of momentum and turbulence.

The data on the modified FFP shown in Fig. 5 also support the idea that X_R is shortened by stronger or more developed canopy turbulence. More notably in the flow2 case, we observe that the locations where linearly interpolated values of FFP cross 50% decrease with increasing upstream canopy length. However, the number of experimental cases as well as the streamwise resolution of the velocity measurement points are too sparse to make these observations conclusive. To confirm the impact of canopy length on FFP-based X_R , additional studies will be needed.

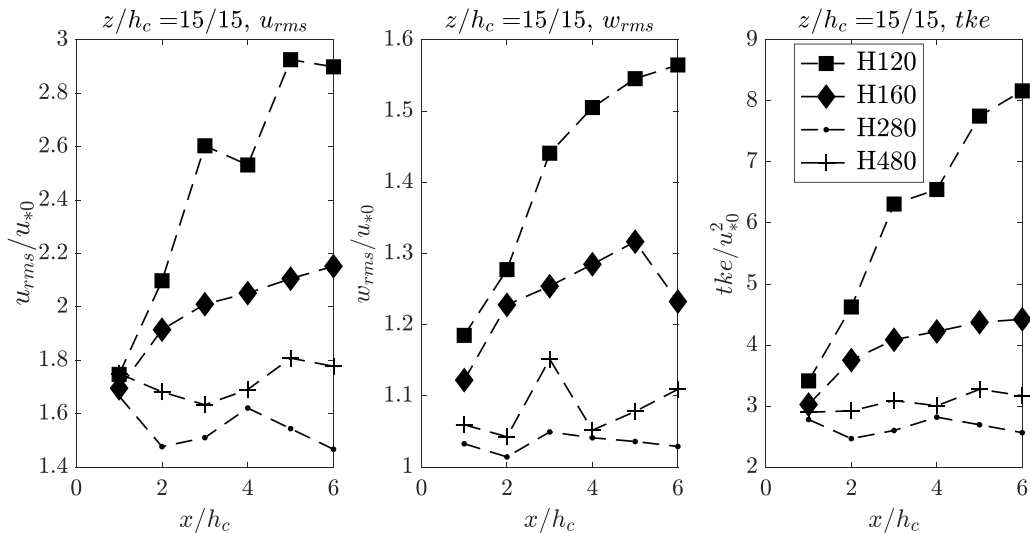


FIG. 13. Turbulence quantities (rms streamwise and vertical velocities, and tke) measured about the canopy height for different homogenous cases of different canopy lengths. The statistics are plotted against downstream distance from the canopy trailing edge.

C. Turbulent wake development

If the structures that impact the wake dynamics are dependent on the turbulence development length, there should be an asymptotic limit at which longer canopy lengths stop impacting the wake separation and reattachment. This is because the structures and corresponding turbulence intensities above the canopy reach a fixed size by a certain length X_* . In this section we look at how the turbulence initial conditions impact the “turbulent wake” often found downstream of canopy edges. As discussed in the Introduction, numerous studies find that RS and tke near the canopy height display a nonmonotonic trend with downstream distance [2,24,27,31], with the turbulence initially increasing to a peak before decreasing. This enhanced turbulence in the wake is thought to be induced by the flow separation and the resulting turbulent stresses. Folkard [2] suggested that the turbulence in the region before the peak ($x = L_w$) is characterized by stronger production than dissipation, with the production and dissipation being in balance at the peak, and with the dissipation dominating thereafter.

However, we find in our studies that this nonmonotonic trend is not observable downstream for all canopy cases. In Fig. 13, we plot the streamwise and vertical root-mean-squared (rms) velocities, and the tke at the canopy height with distance downstream in the wake region. Four of the homogeneous cases are presented: $H120$, $H160$, $H280$, and $H480$. The turbulence quantities are normalized by the initial friction velocity u_{*0} found at the start of the gap, at the canopy height (listed on Table I). We find that by $x = 1h_c$ downstream of the canopy edge at the canopy height, u_{rms}/u_{*0} ranges between 1.66 and 1.75 and w_{rms}/u_{*0} ranges between 1.03 and 1.19. Although these values are measured shortly downstream of the canopy (rather than right above) and already impacted by BFS, they are consistent with those found above various canopy shear flows by Ghisalberti [47] ($u_{rms}/u_* = 1.85 \pm 0.15$; $w_{rms}/u_* = 1.09 \pm 0.02$) and also Chen *et al.* [31].

We observe that both the $H120$ and $H160$ cases experience significantly increasing levels of turbulence all the way to $x = 6h_c$. In contrast, the $H280$ and $H480$ cases show no real trends in turbulence intensities with distance downstream. Important to note here is that due to the normalization by initial conditions, the magnitude differences across the different experimental cases are not representative of actual turbulence intensities. The magnitude of the root-mean-squared

velocity fluctuations as well as tke is much greater for the $H280$ and $H480$ cases than for the $H120$ and $H160$ cases.

These trends indicate two characteristics of the turbulent wake region. First, the turbulence in the wake will not grow in intensity if the turbulence from the upstream canopy is fully developed and has reached an asymptotic limit. Studies above canopies have found that when the flow is not fully developed, the turbulence production is greater than the dissipation (from the canopy elements), and the structures and rollers and turbulence grow along the canopy length [1]. We hypothesize that the relative balance between the production and dissipation at the end of the canopy determines the turbulence budget in the wake. Therefore, because the turbulence production and dissipation are already at balance by the canopy end for $L_1 \geq X_*$, the turbulence will not continue to grow. Rather, it will self-sustain for a short distance before decaying as the production decreases and dissipation increases. If, however, the flow is not fully developed (production greater than dissipation) by the end of the canopy, we will see increasing trends in the tke such as in Fig. 13 for the $H120$ and $H160$ cases.

Based on the observed trends, we hypothesize that the strength of the CSD turbulence may alter the extent to which the turbulent wake will grow in intensity due to the BFS. Similar to the turbulent wake found downstream of the separation in the BFS, canopy wakes can have a separation-induced turbulent wake. This is the case described by Folkard [2], in which the short pruned flexible canopy behaved like a solid and no canopy-induced instability was observed. In that case, the rise in tke in the near wake was entirely due to the separation dynamics. However, in our case, the CSD-induced turbulence is strong enough such that additional turbulence produced by BFS is negligible. In the case where the turbulence is fully developed and the separation-induced turbulence is relatively small, no rise in turbulence intensities will be observed, such as in $H280$ and $H480$. Therefore, we hypothesize that depending on the development of canopy-induced turbulence upstream, the turbulent wakes of different canopy systems experience varying contributions of CSD and/or BFS.

D. Reattachment process

The dependence of the reattachment length on the “initial turbulence levels” into the canopy wake helps us understand the process by which the flow reattaches to the bed. Immediately downstream of the canopy, the mean flow profile maintains a mixing-layer-type shape. Shortly after, the turbulent mixing allows the spreading of the mean shear and Reynolds stress, such that both become more uniform over depth. This process results in the transport of both momentum and turbulence to the bed and the formation of the reattachment zone. The intrusion of turbulence into the dead zone of the wake and entrainment of the irrotational fluid into the shear layer could be dependent on either of two possible processes: (1) the spreading of the mixing layer; and (2) the turbulent mixing modulated by the canopy-induced coherent structures. The former is a possibility because while the vertical extent of the mixing layer is constrained within the canopy, it can expand and grow to the bed upon entering the gap or clearing. If the mixing layer spreads at a constant spreading angle from the canopy edge, then the spreading angle would determine where the shear layer and coherent structures are able to reach the bed. However, because we observe that X_{R0} is dependent on the upstream canopy length, we find this to be not the case. If the entrainment rate, and therefore reattachment, were solely dependent on the mixing-layer spread rate, there would be no influence of canopy length on reattachment. This is because the ML spread rate is solely dependent on the mean velocity profile (Brown and Roshko [48]; Winant and Browand [49]). The cases $H160$, $H280$, and $H480$ presented in Figs. 4 and 5 all have fully developed mean velocity profiles. Therefore, they should all exhibit the same ML spread rate and angle. However, we find that the rate of turbulent intrusion to the bed varies across our cases (different X_{R0}), indicating that spreading of the ML is not responsible for the intrusion of turbulence or reattachment to the bed.

The second possible process by which the turbulence is transported to the bed is by turbulent mixing. This would be more consistent with our results because it requires dependency on the

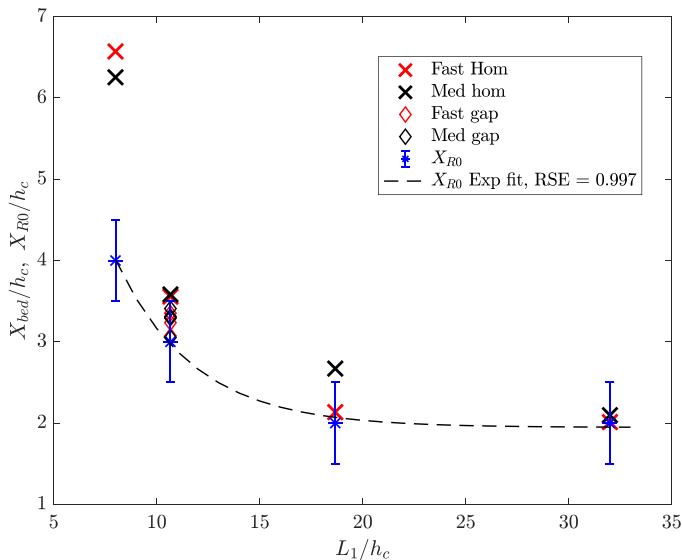


FIG. 14. Scaling of turbulence intrusion to the bed (X_{bed}) is given by the \times and diamond cases. It is plotted against the length of the upstream canopy normalized by the canopy height. The blue plots are the observed X_{R0} for comparison. The error bars are included because the spatial resolution of observing X_{R0} is limited by $1h_c$. The dotted line is an exponential fit to the X_{R0} data with an R -squared error of 0.997.

“initial turbulence levels” at the canopy trailing edge. The longer canopies have larger, more intense turbulent structures with enhanced mixing. We can approximate this by scaling the vertical mixing rate. The time that it takes for the turbulent structures to mix and reach the bed is given by

$$t_{mix} = z_p/u_*0. \quad (3)$$

Over the time t_{mix} , we can approximate the time that the structures travel with the mean velocity \bar{U} in the streamwise direction. This gives us an approximate scaling of the distance it takes for the turbulent structures to reach the bed:

$$X_{bed} = (z_p/u_*)\bar{U}. \quad (4)$$

In Fig. 14, we plot the scaling for X_{bed} for the experimental cases in this study, as well as the values of X_{R0} , the reattachment point, for comparison. The scaling is plotted against the canopy length normalized by the canopy height L_1/h_c . For both the flow1 and flow2 cases, we see that with increasing upstream canopy length, X_{bed} decreases at a decreasing rate. The error bars of $\pm 0.5h_c$ are included because our determination of X_{R0} was limited by the velocity measurements being taken every $1h_c$. We find that our scaling estimate for the streamwise distance for turbulent intrusion to the bed agrees fairly well with the reattachment points found in Sec. III, except for the $H120$ cases. This is most likely because the mean velocity profile in the $H120$ case is not fully developed by the canopy end and other physical processes are still important in this case. While more experimental data points are needed to fully confirm our result, these findings indicate that turbulent mixing induced by canopy instabilities is a dominant contributor to reattachment in the canopy wake. This is reasonable for our canopy system because it is strongly influenced by the CSD and corresponding mixing.

V. CONCLUSIONS

The nature of reattachment of separated flow downstream of canopies has been further refined and characterized in this study. Velocity measurements indicate that both CSD and BFS are present in the mean and turbulent fields prior to reattachment. The flow is initially separated into distinct upper and lower regions, with an interface at the penetration depth z_p . “Reattachment” can be identified near the bed where maximum (reverse) opposing flow is detected in the mean velocity. We define the reattachment zone as beginning at this point X_{R0} and extending to X_{R1} where the flow returns to the exit flow velocity. To characterize the flow throughout the water column above the reattachment zone, we analyzed streamwise and vertical velocity spectra, as well as performed conditional sampling of the turbulence and flow visualization. Over the water column above reattachment, mixing and entrainment of both momentum and turbulence allow the two layers to become less distinct with distance downstream.

In contrast to the BFS flow, mixing of the two layers is strongly influenced by large coherent structures that originate from the upstream canopy. While scales corresponding to both canopy shear and separation are observed, the former dominates the mixing and entrainment in the system and we observe that large periodic structures from the upstream canopies modulate the reattachment. Furthermore, the rate of mixing, and therefore reattachment, depends significantly on the development of the Kelvin-Helmholtz structures (due to canopy-shear) upstream. Shorter canopies have lower turbulence levels at the canopy ends resulting in longer reattachment lengths. Longer canopies (with an asymptotic limit for fully developed flow) result in larger KH structures and stronger turbulence levels that shorten the reattachment length. Additionally, if the turbulence is fully developed by the canopy’s edge, a turbulent wake does not develop downstream (nonmonotonic peak in RS). That is, if the canopy-induced turbulence is strong enough, any additional turbulence enhanced by separation at the canopy edge is negligible. We find that scaling of the mixing rate based on the friction velocity (u_{*0}) of the upstream canopy gives a good estimate of the length required for flow reattachment [Eq. (4)] that matches observed X_{R0} .

While this study improves on the understanding of canopy flow reattachment, the limitations of single-point measurements restrict both spatial resolution and statistical analyses. Additional studies with higher streamwise spatial resolution will help in locating the reattachment more accurately. It would also be worthwhile to compare the behavior observed in our studies to others in which the canopies behave more like a BFS. However, the results from the study signify that canopy characteristics and their impact on the mean and turbulent flow can have strong impact on wake dynamics in a range of canopy systems.

ACKNOWLEDGMENTS

We gratefully acknowledge the support of the Stanford CEE graduate fellowship, Stanford CEE Leavell fellowship, and Stanford graduate fellowship.

-
- [1] M. Ghisalberti and H. M. Nepf, The limited growth of vegetated shear layers, [Water Resour. Res.](#) **40**, W07502 (2004).
 - [2] A. M. Folkard, Hydrodynamics of model *Posidonia oceanica* patches in shallow water, [Limnol. Oceanogr.](#) **50**, 1592 (2005).
 - [3] A. Maltese, E. Cox, A. M. Folkard, G. Ciraolo, G. La Loggia, and G. Lombardo, Laboratory measurements of flow and turbulence: In discontinuous distributions of ligulate seagrass, [J. Hydraul. Eng.](#) **133**, 750 (2007).
 - [4] C. A. O’Riordan, S. G. Monismith, and J. R. Koseff, The effect of bivalve excurrent jet dynamics on mass transfer in a benthic boundary layer, [Limnol. Oceanogr.](#) **40**, 330 (1995).

- [5] A. M. Folkard and J. C. Gascoigne, Hydrodynamics of discontinuous mussel beds: Laboratory flume simulations, *J. Sea Res.* **62**, 250 (2009).
- [6] S. G. Monismith, Hydrodynamics of coral reefs, *Annu. Rev. Fluid Mech.* **39**, 37 (2007).
- [7] J. J. Finnigan, R. H. Shaw, and E. G. Patton, Turbulence structure above a vegetation canopy, *J. Fluid Mech.* **637**, 387 (2009).
- [8] M. R. Raupach, J. J. Finnigan, and Y. Brunet, Coherent eddies and turbulence in vegetation canopies: The mixing-layer analogy, *Boundary Layer Meteorol.* **78**, 351 (1996).
- [9] W. Zhu, R. van Hout, and J. Katz, PIV measurements in the atmospheric boundary layer within and above a mature corn canopy. Part II: Quadrant-hole analysis, *J. Atmos. Sci.* **64**, 2825 (2007).
- [10] E. Follett, M. Chamecki, and H. Nepf, Evaluation of a random displacement model for predicting particle escape from canopies using a simple eddy diffusivity model, *Agric. For. Meteorol.* **224**, 40 (2016).
- [11] T. R. Oke, Street design and urban canopy layer climate, *Energy Build.* **11**, 103 (1988).
- [12] O. Coceal and S. E. Belcher, Mean winds through an inhomogeneous urban canopy, *Boundary Layer Meteorol.* **115**, 47 (2005).
- [13] H. M. Nepf, Flow and transport in regions with aquatic vegetation, *Annu. Rev. Fluid Mech.* **44**, 123 (2011).
- [14] A. C. Ortiz, A. Ashton, and H. Nepf, Mean and turbulent velocity fields near rigid and flexible plants and the implications for deposition, *J. Geophys. Res.: Earth Surf.* **118**, 2585 (2013).
- [15] E. M. Follett and H. M. Nepf, Sediment patterns near a model patch of reedy emergent vegetation, *Geomorphology* **179**, 141 (2012).
- [16] J. Q. Yang, H. Chung, and H. M. Nepf, The onset of sediment transport in vegetated channels predicted by turbulent kinetic energy, *Geophys. Res. Lett.* **43**, 11,261 (2016).
- [17] M. Ghisalberti and H. M. Nepf, Mixing layers and coherent structures in vegetated aquatic flows, *J. Geophys. Res.* **107**, 3-1-3-11 (2002).
- [18] M. Ghisalberti and H. Nepf, Mass transport in vegetated shear flows, *Environ. Fluid Mech.* **5**, 527 (2005).
- [19] M. Ghisalberti and H. Nepf, The structure of the shear layer in flows over rigid and flexible canopies, *Environ. Fluid Mech.* **6**, 277 (2006).
- [20] H. M. Nepf and E. R. Vivoni, Flow structure in depth-limited, vegetated flow, *J. Geophys. Res.: Oceans* **105**, 28547 (2000).
- [21] M. Detto, G. G. Katul, M. Siqueira, J. Y. Juang, and P. Stoy, The structure of turbulence near a tall forest edge: The backward-facing step flow analogy revisited, *Ecol. Appl.* **18**, 1420 (2008).
- [22] A. Montakhab, B. Yusuf, A. H. Ghazali, and T. A. Mohamed, Flow and sediment transport in vegetated waterways: A review, *Rev. Environ. Sci. Biotechnol.* **11**, 275 (2012).
- [23] M. Cassiani, G. G. Katul, and J. D. Albertson, The effects of canopy leaf area index on airflow across forest edges: Large-eddy simulation and analytical results, *Boundary Layer Meteorol.* **126**, 433 (2008).
- [24] F. Zarama, Development of turbulence downstream of submerged aquatic vegetation, Ph.D. thesis, Stanford University, 2017.
- [25] N. Anjum and N. Tanaka, Investigating the turbulent flow behaviour through partially distributed discontinuous rigid vegetation in an open channel, *River Res. Appl.* **36**, 1701 (2020).
- [26] A. M. Hamed, A. M. Peterlein, and I. Speck, Characteristics of the turbulent flow within short canopy gaps, *Phys. Rev. Fluids* **5**, 123801 (2020).
- [27] H. Chung, T. Mandel, F. Zarama, and J. R. Koseff, Local and nonlocal impacts of gaps on submerged canopy flow, *Water Resour. Res.* **57** (2021).
- [28] I. Tani, Effect of Two-Dimensional and Isolated Roughness on Laminar Flow, in *Boundary Layer and Flow Control* (Elsevier, Amsterdam, 1961), pp. 637–656.
- [29] J. K. Eaton and J. P. Johnston, Turbulent flow reattachment: An experimental study of the flow and structure behind a backward-facing step., Ph.D. thesis, Mechanical Engineering MD-39, Stanford University, 1980.
- [30] C. Chandrsuda, A reattaching turbulent shear layer in incompressible flow, Ph.D. thesis, Imperial College of Science and Technology, 1975.
- [31] Z. Chen, C. Jiang, and H. Nepf, Flow adjustment at the leading edge of a submerged aquatic canopy, *Water Resour. Res.* **49**, 5537 (2013).

- [32] A. M. Hamed, M. J. Sadowski, H. M. Nepf, and L. P. Chamorro, Impact of height heterogeneity on canopy turbulence, *J. Fluid Mech.* **813**, 1176 (2017).
- [33] S. Fontan, G. G. Katul, D. Poggi, C. Manes, and L. Ridolfi, Flume experiments on turbulent flows across gaps of permeable and impermeable boundaries, *Boundary Layer Meteorol.* **147**, 21 (2012).
- [34] A. Kurtis, *Newsom's Wildfire Plan May Have A Problem When It Comes To Fighting Big Blazes* (San Francisco Chronicle, 2021).
- [35] R. V. Westphal and J. P. Johnston, Effect of initial conditions on turbulent reattachment downstream of a backward-facing step, *AIAA J.* **22**, (1984).
- [36] C. Chandrsuda and P. Bradshaw, Turbulence structure of a reattaching mixing layer, *J. Fluid Mech.* **110**, 171 (1981).
- [37] P. Bradshaw and D. F. Wong, The reattachment and relaxation of a turbulent shear layer, *J. Fluid Mech.* **52**, 113 (1972).
- [38] J. K. Eaton and J. P. Johnston, A review of research on subsonic turbulent flow reattachment, *AIAA J.* **19**, 1093 (1981).
- [39] T. R. Troutt, B. Scheelke, and T. R. Norman, Organized structures in a reattaching separated flow field, *J. Fluid Mech.* **143**, 413 (1984).
- [40] X. Ma and A. Schröder, Analysis of flapping motion of reattaching shear layer behind a two-dimensional backward-facing step, *Phys. Fluids* **29**, 115104 (2017).
- [41] A. Dejoan and M. A. Leschziner, Large eddy simulation of periodically perturbed separated flow over a backward-facing step, *Int. J. Heat Fluid Flow* **25**, 581 (2004).
- [42] M. M. Rogers and R. D. Moser, Direct simulation of a self-similar turbulent mixing layer, *Phys. Fluids* **6**, 903 (1994).
- [43] T. L. Mandel, S. Gakhar, H. Chung, I. Rosenzweig, and J. R. Koseff, On the surface expression of a canopy-generated shear instability, *J. Fluid Mech.* **867**, 633 (2019).
- [44] P. E. Dimotakis and G. L. Brown, The mixing layer at high Reynolds number: Large-structure dynamics and entrainment, *J. Fluid Mech.* **78**, 535 (1976).
- [45] F. K. Browand and C. D. Winant, Laboratory observations of shear-layer instability in a stratified fluid, *Boundary Layer Meteorol.* **5**, 67 (1973).
- [46] V. De Brederode and P. Bradshaw, Influence of the side walls on the turbulent center-plane boundary-layer in a square duct, *J. Fluids Eng.* **100**, 91 (1978).
- [47] M. Ghisalberti and H. Nepf, Shallow flows over a permeable medium: The hydrodynamics of submerged aquatic canopies, *Transp. Porous Media* **78**, 309 (2009).
- [48] G. Brown and A. Roshko, On density effects and large structure in turbulent mixing layers, *J. Fluid Mech.* **64**, 775 (1974).
- [49] C. Winant and F. Browand, Vortex pairing: The mechanism of turbulent mixing-layer growth at moderate Reynolds number, *J. Fluid Mech.* **63**, 237 (1974).